

Fotokatalytisk hydrogenproduksjon gjennom fotoreforming av hydrokarboner

Eirik Djuve

Industriell kjemi og bioteknologi

Innlevert: juni 2013

Hovedveileder: Magnus Rønning, IKP

Medveileder: Charitha Udani, IKP

Norges teknisk-naturvitenskapelige universitet
Institutt for kjemisk prosess teknologi

Preface

This study was carried out as a master thesis for the Department of Chemical Engineering at the Norwegian University of Science and Technology (NTNU) during the spring of 2013. My supervisor was Professor Magnus Rønning and co-advisor was PhD candidate Charitha Udani.

I chose this project because i wanted to learn something new and exciting and because I like the idea of contributing (even so little) to the development of environmental-friendly energy solutions. The goal of the project was to understand and optimize the production of hydrogen from a mixture of water and methanol, using UV-light as energy input and copper loaded titanium oxide as a photocatalyst for the process. A practical routine for obtaining reproducible results had to be refined and optimization of the process was performed mainly by tuning the catalyst loading in the reactor and the copper content in the photocatalyst.

I would like to thank my supervisors for giving me help, inspiration, and training in addition to contributing to a great working environment which made this project a positive experience for me. I would also like to thank Karin Wiggen for teaching me how to use the BET instrument, Harry Brun for teaching me about the correct use of the gas equipment and Arne Fossum for providing the much needed chemicals and equipment.

I declare that this is an independent work according to the exam regulations of the Norwegian University of Science and Technology (NTNU).

Eirik Djuve

Sammendrag

Hensikten med dette prosjektet var å undersøke Cu–TiO₂ som fotokatalysator for fotoreforming av metanol. Dette er en prosess der hydrogen blir produsert fra metanol i vannløsning ved hjelp av UV-lys og en fotokatalysator. Denne prosessen renses også vannet, men for at prosessen skal få noen realistisk nytte må den optimeres og de dyre edelmetallene som for øyeblikket gir best resultater som ko-katalysatorer, må byttes ut. Kobber/kobberoksid er valgt som ko-katalysator i dette prosjektet fordi det er relativt billig og tilgjengelig. Denne prosessen kan gjøres miljøvennlig og CO₂ nøytral ved å bruke sola som lyskilde og biomasse som hydrokarbonkilde.

En rekke fotoreforming eksperimenter ble utført for å kartlegge kobber-innholdet sin effekt på aktiviteten til fotokatalysatoren og for å finne det optimale kobber innholdet. Videre ble det eksperimentert med å bruke forskjellige mengder katalysator i reaktoren for å finne ut hvilken effekt katalysatormengde har på hydrogen produksjonen. Deaktivering ble også undersøkt ved å se på den fallende hydrogenproduksjon og ved å forsøke å reaktivere katalysatoren. Til slutt ble det utført BET analyse på de forskjellige katalysatorene for å finne ut hvilken effekt kobber innholdet og produksjonsmetoden har på overflate arealet til katalysator pulveret.

Fem forskjellige katalysatorer ble fremstilt ved *Incipient Wetness Impregnation* (IWI) metoden med forskjellige kobber-innhold mellom 0 og 10 masseprosent. Det var overraskende liten forskjell på de forskjellige fotokatalysatorenes evne til å produsere hydrogen, med unntak av den kobberfrie katalysatoren som ikke produserte noen detekterbar mengde i det hele tatt. Ved små mengder katalysator ble hydrogen produksjonen funnet til å være tilnærmet lineært avhengig av katalysormengden i reaktoren, mens ved større mengder flatet kurven ut. Den optimale katalysatormengden for dette systemet ble oppdaget til å være på rundt 500 mg, som tilsvarer 1 g/l. Ved denne katalysatormengden ble maksimale hydrogenproduksjonen målt til å være 3,05 mmol h⁻¹ g_{cat.}⁻¹ ved bruk av 10 m.% CuO på TiO₂ og energieffektiviteten ble beregnet til å være på 0.41 %.

Ved å fornye væskefasen til systemet ble mye av den tapte hydrogenproduksjon gjenopprettet, noe som tyder på at akkumulering av biprodukter er den dominerende årsaken til deaktivering. Det ble også oppdaget at fotoreformings reaksjonen fører til en viss redusering av CuO til metallisk Cu. Videre ble det ved BET målinger også oppdaget at selve IWI metoden etterfulgt av kalsinering ikke hadde noen innvirkning på det spesifikke overflatearealet til fotokatalysatoren, mens økende innhold av CuO reduserte det spesifikke overflatearealet.

Abstract

The purpose of this study was to investigate and optimize photoreforming of methanol as an environmental-friendly way to produce hydrogen as a by-product from cleaning water. In order to scale up this process in a realistic manner and make it globally available, the expensive noble metals currently used in the TiO₂ based photocatalyst has to be replaced by cheaper alternatives like CuO which was chosen in this project.

In this study, the impact of the copper content in the catalyst was investigated along with the catalyst loading in the photoreactor. Deactivation and reactivation was briefly studied and BET surface area measurements were performed to correlate the effect of copper content on the surface area of the catalyst.

Five different catalysts were prepared by using the incipient wetness (IWI) method, having a copper content of 0 wt.% , 1 wt.% , 5 wt.% , 7.5 wt.% and 10 wt.% respectively. The activity of these photocatalysts were tested in a photoreforming process where a mixture of 250 ml water and 250 ml methanol was converted to H₂ gas and CO₂ using UVC-light at 254 nm. The photocatalyst without copper did not produce any detectable amounts of H₂ gas, but the peak hydrogen production rate among the other catalysts was very even. The catalyst containing 10 wt.% copper did achieve the highest hydrogen generation rate, but the difference to the other catalysts were marginal so nothing can be concluded due to random measurement errors.

Several photoreforming experiments were conducted with different catalyst loadings in order to investigate the relationship between hydrogen generation and catalyst loading. At very low catalyst loadings, the relationship between catalyst loading and hydrogen generation seemed almost linear and at higher loadings the curve flattened out. It was discovered that the catalyst saturation point for this system was at about 500 mg, meaning that adding more photocatalyst after this point would not further increase the hydrogen generation rate. At this catalyst loading, the 10 wt.% CuO on TiO produced a maximum of 3.05 mmol H₂ h⁻¹ g_{cat.}⁻¹ with a calculated quantum yield of 0.41 %

Deactivation was also briefly studied by registering the decay in hydrogen generation over time and by attempting to reactivate the catalyst. Reactivation by hydrogen reduction did not have any notable effect, but refreshment of the liquid phase was highly effective in recovering the lost hydrogen generation rate. This suggests that accumulation of by-products is the most significant source of deactivation. It was also discovered that deactivation of the catalyst by reduction of CuO to metallic Cu takes place, but the actual extent and impact of this effect was not quantified.

The IWI method produced a catalyst where the particles tend to agglomerate to a varying degree. Because of this, getting reproducible results during the photoreforming experiments proved to be a real challenge. The solution to this problem was to make the particle size as uniform as possible by repeated steps of crushing and sieving. BET experiments showed that the specific surface area of the TiO₂ particles was unaffected by the IWI method and the calcination treatment. The specific surface area was also found to decrease when TiO₂ was loaded with CuO, meaning that a higher copper loading caused a lower specific surface area.

Contents

Preface	i
Norsk sammendrag	iii
Abstract	v
Contents	1
List of symbols and abbreviations	3
1 Introduction	4
2 Theory and background information	6
2.1 What is a photocatalyst?	6
2.2 The history of photocatalysis	7
2.3 How photocatalysts work	8
2.4 Photoreforming	9
2.5 Commercial applications of TiO ₂ photocatalysis today	15
2.6 General properties of TiO ₂ and modifications	17
2.6.1 Strategies for improving titania's photoactivity	19
2.6.2 TiO ₂ loaded with copper and other co-catalysts	22
2.7 Alternatives to titania	26
2.8 Fabrication methods of TiO ₂ based photocatalysts	28
2.8.1 Incipient wetness impregnation (IWI)	28
2.8.2 Calcination	28
2.8.3 Deposition precipitation method	29
2.8.4 Photo deposition method	29
2.8.5 Sol-gel method	29
2.9 Deactivation in photoreforming and water splitting	31
2.10 Surface area measurement by BET analysis	32
3 Experimental	33
3.1 Preperation of the catalyst	33
3.2 Activity measurements	35
3.3 The challenge of obtaining reproducible results	36
3.4 Reactivation attempts	39
3.5 BET measurements	39
4 Results and discussion	40
4.1 Activity measurments	40
4.1.1 The effect of catalyst loading on hydrogen generation	40
4.1.2 The effect of copper content on the photocatalytic activity of Cu–TiO ₂	43
4.2 Catalyst deactivation and reactivation attempts	45
4.3 Additional observations	48
4.4 Choosing the appropriate values to report	51
4.5 BET results	53

5	Conclusions	54
6	Future work	55
	References	56
	Appendix	I
	Appendix A: Calculation examples and assumptions	I
	Calculations regarding catalyst preparation	I
	Calculating the quantum yield	I
	Quantifying the reproducibility by calculating relative errors	II
	Thermodynamics: Finding the temperature needed to spontaneously form significant amounts of Cu_2O	III
	Appendix B: List of chemicals	IV
	Appendix C: BET data	V
	Appendix D: HSE and risk assessment	VIII
	Explanations	VIII
	Hazardous activity identification process	IX
	Risk assessment	XII
	Chemical data sheets	XIV

List of symbols and abbreviations

Symbol/abbreviation	Meaning	Unit
TW	Terawatt, 1 TW= 1×10^{12} watts	W, TW
UV-rays	Ultra violet rays ($10 \text{ nm} < \lambda < 400 \text{ nm}$)	-
λ	Wavelength of electromagnetic waves	m, nm
IUPAC	International Union of Pure and Applied Chemistry	-
BET	A characterisation method, see page 32	-
VB	Valence band	-
CB	Conduction band	-
Θ	Radiant flux of light	W, lm (lumen)
VOC	Volatile organic compound	-
eV	Electron volts, 1 eV= 1.9×10^{-19} V	eV, V
Turbidity	The cloudiness or haziness of a fluid	NTU
M	molar concentration	mol/l
SCE	Saturated calomel electrode(a reference electrode)	-
HOMO	Highest occupied molecular orbital	-
LUMO	lowest unoccupied molecular orbital	-
P	Pressure	mmHg, bar
(aq)	Dissolved in water	-
(s)	solid state	-
(g)	gaseous state	-
IWI	Incipient wetness impregnation	-
ΔH_{298}°	Standard enthalpy of reaction	kJ/mol
DP	Deposition precipitation	-
PD	Photo deposition	-
STP	Standard temperature and pressure	-
V	Volume	ml, l, cm^3 at STP
V_m	Adsorbed gas volume by monolayer coverage	cm^3 at STP
T	Temperature	$^{\circ}\text{C}$, K
ΔH_{ads}	Heat of adsorption	kJ/mol
χ	$\frac{\Delta H_{ads-layer 1}}{\Delta H_{ads-layer 2}}$	-
P_0	saturation pressure	bar, mmHg
m, wt.	Mass, weight	mg, g
GC	Gas chromatograph	-

1 Introduction

Today we live in a world where the demand for energy continues to grow while our reservoirs of fossil fuel are slowly being depleted. This calls for alternative energy sources, where renewable energy is highly preferred. Solar energy has the biggest theoretical potential of 600 TW [1], which is 40 times as big as the total world consumption of 15 TW [2]. This means that if only a few percent of this energy could be successfully harvested, it would supply the entire human population with enough energy. The traditional scientific way of transforming radiation from the sun into highly applicable electrical energy, is by the use of solar cells. When solar cells are used, the electric energy produced is usually used directly, being saved in batteries or used to split water into oxygen and hydrogen by electrolysis. The latter is an example of how hydrogen can be used as an energy carrier, where the energy from the hydrogen can be regained in a fuel cell or by combustion. What separates an energy carrier from an energy source is that an energy carrier needs energy input and is only used to store energy for a limited amount of time.

Today, most of the hydrogen produced in the world come from steam reforming of hydrocarbons from natural gas which is a non-renewable source [3]. This is a complicated and energy demanding process which leads to emissions of CO_2 and other greenhouse gasses. Hydrogen may also be made from renewable biomass through pyrolysis, but this process is energy demanding which hampers the total energy efficiency [4]. Both of these processes produce CO as one of the by-products, which is a problem if the hydrogen is to be used in a fuel cell. The catalyst used in fuel cells is easily poisoned by CO, so if this gas mixture is to be used in a fuel cell the CO has to be removed first. This is why the clean hydrogen produced by electrolysis of water is preferred in fuel cells [5]

Water electrolysis powered by solar cells is not the only route to produce hydrogen from solar energy. Hydrogen gas can also be produced directly from water through photocatalytic water splitting, omitting the electrolysis step. In this process the water is mixed with a catalyst powder, usually titanium dioxide with a co-catalyst. When this mixture is irradiated with UV-rays, the titanium oxide becomes active and some water splits into hydrogen and oxygen. These UV-rays should ideally come from the sun, in order to make the process sustainable. Because the catalyst needs to be irradiated with photons to become active, it is called a photocatalyst.

The rate of hydrogen production may be increased by adding a sacrificial agent to the mixture. A sacrificial agent is usually an oxygenated organic compound like sugars, alcohols and organic acids. When such compounds are added to the reaction mixture, the process is called photoreforming and the sacrificial agents are converted to CO_2 along with H_2 gas. These compounds may come from renewable sources like plants and general vegetation, or they may come from wastewater. For example, the sewage from the food industry is rich in water-soluble carbohydrates [6]. This means that photoreforming may be utilized as a process to cleanse water using sunlight, while even producing hydrogen as a wanted by-product.

Because areas having a poor water supply often have plenty of sunlight, this technology has great potential to be a good solution when it has matured. The process is also in principle CO₂ neutral as long as the organic compounds comes from renewable sources like biomass and not from fossil ones. Because of ever continuing population growth, experts think that pure drinking water and energy will be the most scarce resources in the future [7]. Photocatalysis might offer a solution to this problem, as it combines the earth's most abundant energy source (the sun) with the most abundant resource (water) and convert it into applicable energy and pure drinking water.

Unfortunately the development of the photocatalysis field has not yet come to a point where this technology is widely applicable. Today's photocatalysts are constrained by the fact that most of them can only utilize a small part of the solar spectrum and the overall efficiency is quite low. If hydrogen technology is to be adopted by the society, new infrastructure is needed along with new technologies for sustainable hydrogen storage and distribution [8].

This project focuses on copper loaded TiO₂ which is one of the most cost effective photo catalyst developed so far. Some of the goals are to find the optimum copper loading, to find the optimum catalyst mass to use for experiments and to develop a routine to ensure that the obtained activity measurements are repeatable. Deactivation will also be studied and the different catalysts will be analysed with a BET instrument to correlate the specific surface area to the copper content in the photocatalysts.

2 Theory and background information

2.1 What is a photocatalyst?

IUPAC defines photocatalyst as "catalyst able to produce, upon absorption of light, chemical transformations of the reaction partners. The excited state of the photocatalyst repeatedly interacts with the reaction partners forming reaction intermediates and regenerates itself after each cycle of such interactions." [9]. The definition of a catalyst is a substance that increases the rate of a chemical reaction without being consumed. Simply put, a photocatalyst is a catalyst that becomes active under/during the irradiation of photons which may come naturally from the sun or from man-made light bulbs or lamps. The adsorbed photons excites electrons from the valence band (VB) to the conduction band (CB) in the photocatalytic material, producing an oxidative hole and a reducing electron. Because photocatalysts may utilize photons as an energy input, they are able to drive uphill reactions that are otherwise not thermodynamically favourable at the current conditions. This marks a clear distinction from normal catalysts, which can never drive uphill reactions or change the equilibrium composition of a chemical mixture. The conceptual difference between a catalyst and a photocatalyst is illustrated in figure 1 below.

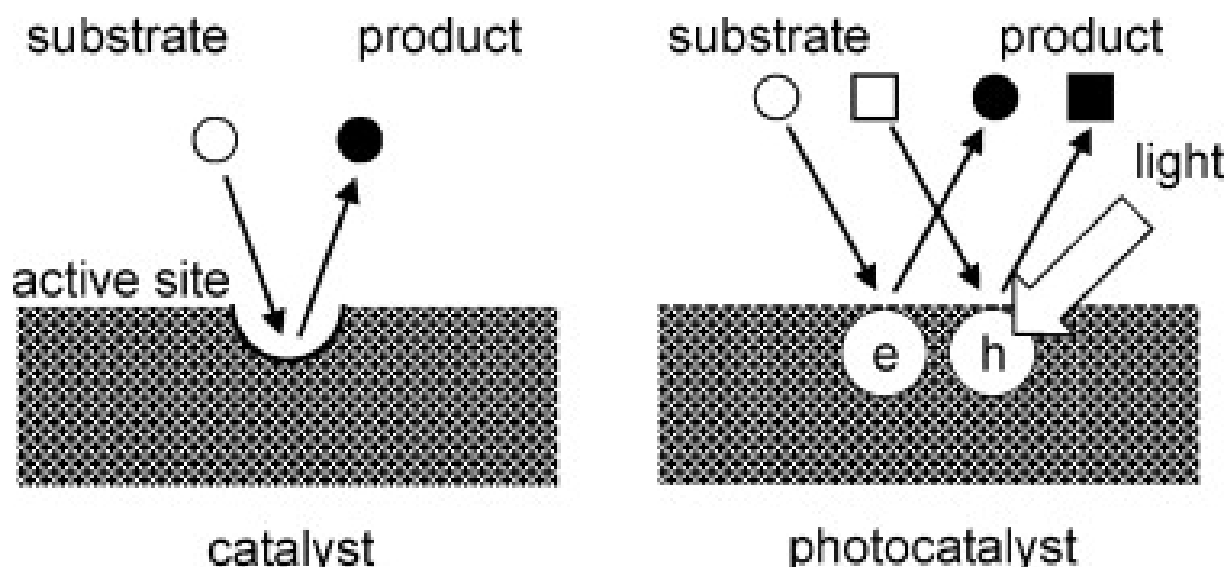


Figure 1: The difference in concepts between catalysis and photocatalysis. Note that the term "active site" is not used on the photocatalysts because it is inappropriate [10].

The rate of catalytic reaction on a photocatalyst is predominantly governed by the number of active sites that are irradiated with light and the light intensity. The dark side of a photocatalyst does not contribute to the reaction rate so usage of the term "active site" is therefore inappropriate [10].

2.2 The history of photocatalysis

Although the field of photocatalysis is relatively new and unknown to most people, it actually has roots reaching more than 80 years back in time. The Swiss were some of the first to report photocatalytic activity, starting as early as in 1921. A Swiss named Renz reported that titania would change colors when in contact with organic compounds while being exposed to sunlight. The color changed from white to grey, blue or even black when irradiated, and this was believed to happen due to partial oxidation of the oxide. Similar phenomena were also discovered with oxides of cerium, niobium and tantalum. In 1924, Baur and Perret at the Swiss Federal Institute of Technology reported that photocatalytic deposition of metallic silver occurred when ZnO was in contact with a silver salt during exposure to sunlight. Even at this early date, the authors suspected that both reduction and oxidation were occurring at the same time. In 1932 Renz reported that the same would happen to gold on TiO₂ and Nb₂O₅, and already in 1927 scientists made H₂O₂ from methanol on a ZnO photocatalyst [11].

In the late 1930s the chalk formation on paints was studied extensively and it was confirmed that the cause of this phenomenon is related to titania's photocatalytic activity. In the late 1950s, Russian scientists discovered an important difference between photocatalytic properties of ZnO and TiO₂. It was found that TiO₂ was able to fully oxidise H₂O to O₂ but ZnO could not oxidise it further than to H₂O₂. This is probably one of the factors that caused TiO₂ to exceed ZnO in popularity in the 1960s. The Japanese scientists Kato and Mashio discovered in 1964 that the anatase allotrope of TiO₂ is more active than rutile during photocatalytic oxidation of organic molecules.

An important breakthrough happened in 1972 when photocatalytic water splitting was reported for the first time by Fujishima and Honda. They used a titanium electrode to split water into hydrogen and oxygen through photoelectrochemistry, and this method of water splitting was named "The Honda-Fujishima effect". This discovery put photocatalysis in the spotlight and helped accelerate the study of the field [10] [12]. Today technology based on photocatalysis is being used to purify water and air through oxidation of organic compounds, in self-cleaning surfaces, in anti-fogging mirrors and sterilization of tiles among others.

2.3 How photocatalysts work

The main point of developing photocatalysts is usually to utilize the sunlight in some way, which is why the solar spectrum will be presented first in this section. The solar spectrum is shown in figure 2 below.

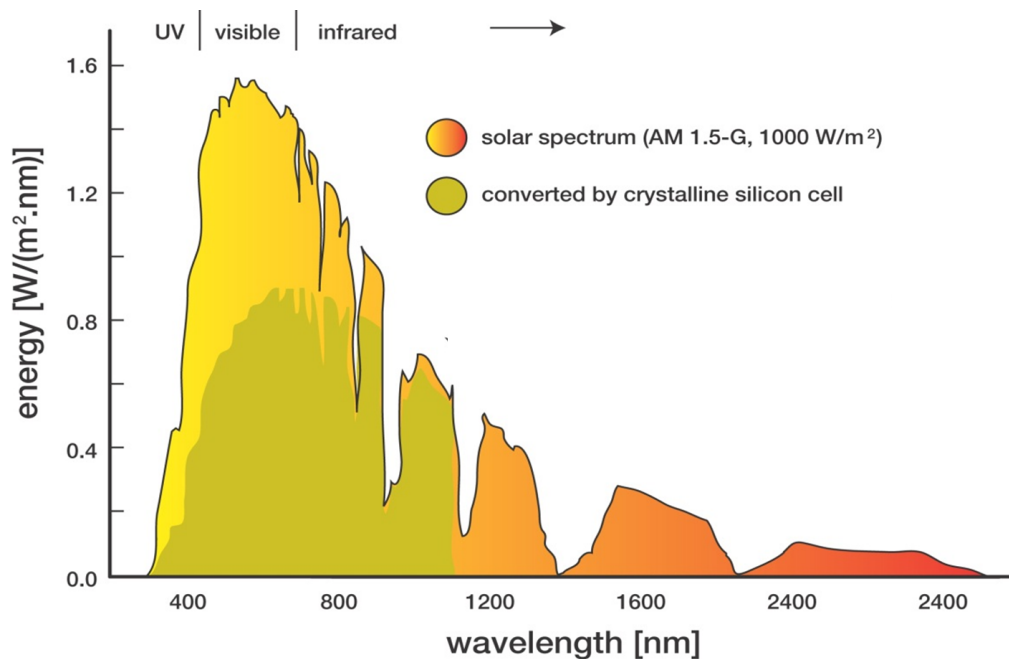


Figure 2: The figure shows the spectrum from the sun [13].

As one can see in the figure, the solar spectrum consists of 5% UV light, 43% visible light and 52% infra-red light. A major challenge today is to develop photocatalysts which can utilize more than just the UV part of the spectrum.

Photocatalysts are semiconductors where a metal or a metal oxide may be added as a co-catalyst for increased activity. Semiconductors have a band gap between their valence band (VB) and their conduction band (CB) which is the key to their photocatalytic activity. When a photon is adsorbed by the semiconductor, it may excite an electron from the valence band to the conduction band if the photon has the sufficient energy to overcome the bandgap. The excited electron will leave an electron hole in the valence band which has oxidizing properties, whereas the electron in the conduction band is able to participate in a reduction. Because of this electron-hole redox couple, the photocatalyst may drive a number of reactions to happen including the splitting of water and oxidation of organic compounds [14].

The position of the valence band and the conduction band of a semiconductor is a very important factor in determining the potential a semiconductor has as a possible photocatalyst. For photocatalytic water splitting, the excited electron in the conduction band needs to have a lower electrode potential than the H_2 and H^+ redox couple in order to perform a H_2 producing reduction. Another requirement is that the upper level of the valence band has a higher electrode potential than the potential of O_2 formation, making

the oxidation of the oxygen atom in H_2O possible [6]. If the bandgap of the semiconductor is small, it will be less energy demanding for photons to cause an excitation. Because the energy of the photons decrease with increasing wavelength, a photocatalyst having a low bandgap may also utilize light at a higher wavelength such as visible light. There is however a critical drawback to having a small bandgap, which is the fact that electrons and holes will recombine at an increased rate. When such a recombination occurs, no chemical reaction will take place and the photon energy is only converted to heat. This leads to decreased activity, even though a larger part of the sunlight may be used. Because of this, there is a trade-off between increasing the bandgap to stop recombination and narrowing it to harvest more sunlight which has to be balanced for optimization of the photocatalysts. The band positions of some semiconductors are shown in figure 17 on page 27.

2.4 Photoreforming

The main focus of this project is photocatalytic water splitting assisted by methanol. In this process it is in fact mostly the methanol which is converted to H_2 gas and CO_2 while most of the water remain intact. This reaction is called "Photoreforming" and will in principle be CO_2 neutral if the methanol is made from biomass and sunlight is utilized as the source of light. There are several proposed mechanisms for photoreforming reactions which depends on the catalyst used, but here is what most of them have in common:

- A photon is first adsorbed by the semiconductor, causing an electron to be excited from the valence band to the conduction band
- The hole left behind in the valence band reacts with water and forms a hydroxy radical ($\text{OH}\cdot$) and a H^+ ion
- If oxygenated hydrocarbons containing one or several OH groups are present, they will act as a sacrificial agent and react with the hole in water's place forming a H^+ ion and a reactive $\text{R-O}\cdot$ radical
- The oxygenated hydrocarbons and their respective radicals will undergo a series of oxidation reactions with either an electron hole or with another radical, gradually transforming it to CO_2 by either removal of hydrogen atoms or by introduction of oxygen
- The excited electron is transferred to a co-catalyst if present, before it reduces H^+ to H_2 . It can also reduce O_2 to an unstable $\text{O}_2\cdot$ radical
- The end products are always CO_2 , H_2 and sometimes CO in addition to partly oxidized hydrocarbons as by products

Hydrocarbons such as sugars and alcohols, are often called "sacrificial agents" because they are easier to reduce than water which makes them react with the holes in it's place.

A proposed mechanism for photoreforming using a Pt–TiO₂ catalyst is shown below in figure 3 which also illustrates the reaction steps on the previous page.

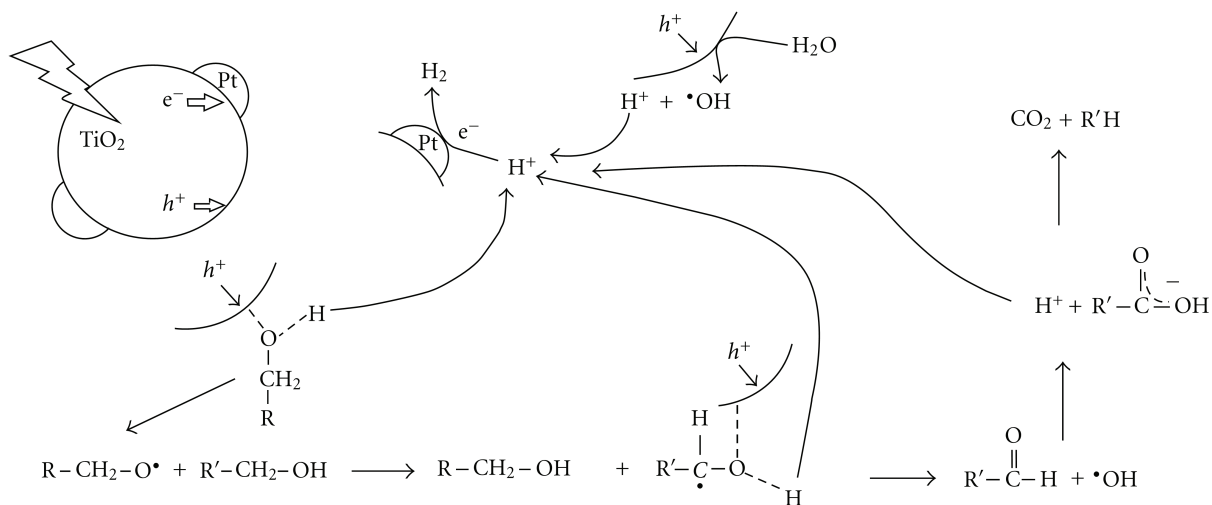


Figure 3: The figure illustrates the reaction steps which are likely to occur during photoreforming [6].

The steps above are the one that drives the reaction forward and produces the desired product. There are however some unwanted side reactions that will decrease the overall efficiency and slow down the hydrogen production rate. These unwanted steps are :

- Recombination of the electron and the hole either on the surface or in the bulk phase
- Back-reaction between oxidized species and an electron
- Back-reaction between reduced species and a hole
- Back-reaction between O₂ and H₂ at the catalyst surface to form water

When optimizing a photocatalyst the aim is to prevent the back-reactions and recombination from happening while maximizing the efficiency of the forward-reaction steps. The time-scales of these processes are different, and this is illustrated in figure 4 below.

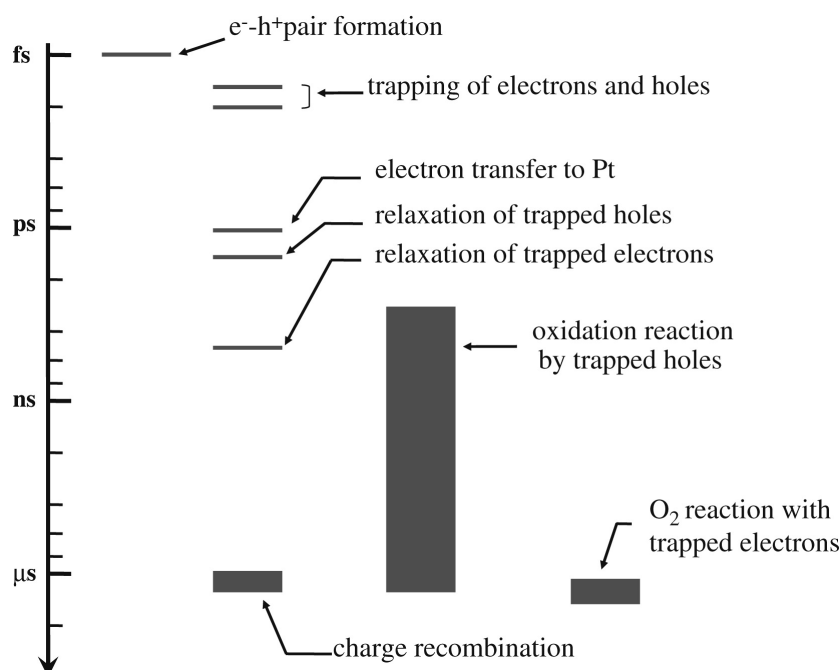


Figure 4: The figure shows time scales of the different processes involved in photocatalysis [15].

As one can see from the figure, electron transfer to a noble metal occurs relatively fast and is an important reason for their effectiveness as co-catalysts. The oxidation reactions with holes is slightly slower but also occurs relatively fast, giving an explanation for the effectiveness of hole scavengers such as methanol. According to Ilenia Rossetti [6] the reduction of H^+ by excited electrons happens much slower than the oxidation of sacrificial agents by holes, actually as slow as in the milliseconds range. Because of this, electrons will accumulate in the photocatalyst and the rate of electron-hole recombination is enhanced until the sum of the reaction rates and recombination rate equals the rate of photogenerated electrons and holes [16].

When it comes to the rate limiting step in photocatalysis, the situation is different from traditional catalysis. In traditional heterogeneous catalysis, the reaction happens stepwise in series where the rate determining step is the slowest one having the highest activation energy. To speed up such a reaction, one has to change the concentrations of the reactants, increase the temperature or make changes to the catalyst that decrease the activation energy of the rate determining step. When these parameters are optimized, the reaction rate will be diffusion controlled and one will have to increase the stirring speed or flow rate to further increase the total reaction rate [17]. In photocatalysis, the situation is different and the reactions may also happen simultaneously in parallel. The activation energy is not overcome by thermal activation like in traditional catalysis, but

by photonic activation [18]. As a consequence, the photocatalytic reaction rate is much less sensitive to changes in temperature compared to thermally activated reactions. In photoreforming, it may be misleading to define one rate determining step because there will usually be several factors that simultaneously affects the total reaction rate. A good way to describe the situation is to define three regimes with respect to photon flux, and describe them thoroughly. The three regimes are illustrated in figure 5 below.

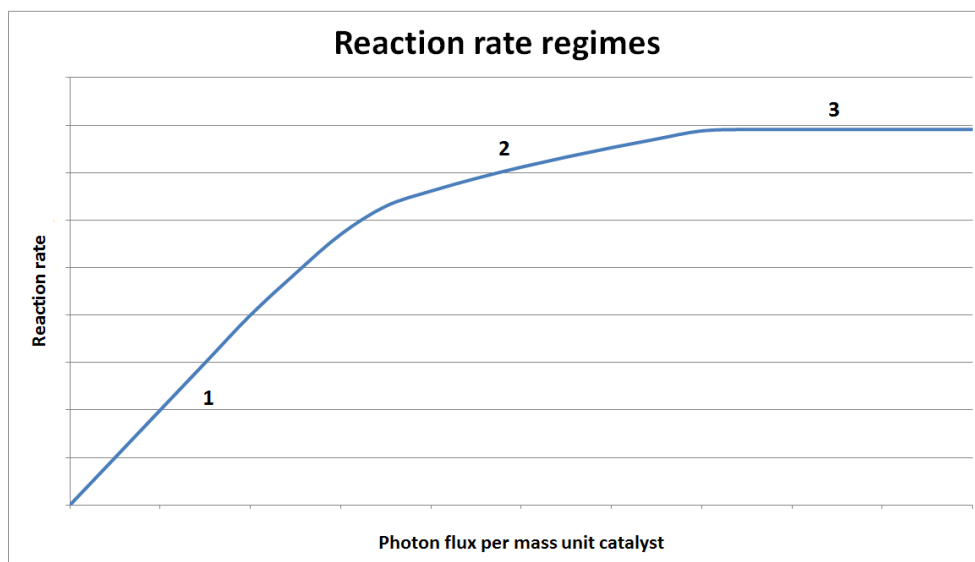


Figure 5: The figure shows how the total reaction rate increases with the light intensity.

J.-M Herrmann [18] describes the first and second regime, while B. Ohtani [10] describes the extreme cases of the first and the third regime. In the first regime, the reaction is light-intensity controlled where the lack of electrons and holes controls the reaction. The reaction rate is proportional to the radiant flux in this regime. The diffusion of substrate to the surface of the photocatalyst particle and the adsorption on to the particles is fast compared to the photogeneration holes and electrons. This is the case for high catalyst loadings where the photons are shared by a great number of catalyst particles, or when a low amount of UV lamps are used which results in low light intensities. In this regime, the reaction rate is proportional to the radiant flux and it can be increased simply by adding more UV-lamps to the set-up.

In the second regime, increasing the photon flux does still increase the reaction rate but the rate of electron excitation (decided by the radiant flux) is now higher than the consumption of electrons by reduction of adsorbed H^+ ions. This causes electrons to accumulate in the bulk TiO_2 phase and H^+ to accumulate on the surface, until the sum of the recombination rate and the reduction rate of H^+ which consumes electrons equals the generation of electrons by photonic excitation. Because the rate of recombination increases with the radiant flux, some photon energy is wasted and the reaction rate's dependence on the light flux starts to fall off. Herrmann argues that the reaction rate at this point is proportional to the square root of the radiant flux ($\sqrt{\Theta}$), but this might not be the case for photoreforming. In his example, the substrate to be reduced and the substrate to be oxidised are independent of each other, but in the case of photoreforming

the substrate to be reduced (H^+) is mainly generated from the sacrificial agent when it is oxidised by holes. In this regime, increasing the concentration of the sacrificial agent will also have a positive effect on the activity.

The third regime occurs when the radiant flux is very high or when the catalyst loading is really low, causing every particle of the photocatalyst to receive an excess of incoming photons. At this point, the total reaction rate is diffusion controlled and the surface reaction happens very rapidly. In this regime, the reaction rate is proportional to the concentration of the sacrificial agent and first-order kinetics is observed [10]. An increase in the radiant flux may in the best case only increase the temperature in the reactor, contributing poorly to boost the reaction rate.

The total reaction rate in a reactor is also a function of the catalyst loading. Herrmann [18] reports that there is a linear relationship between the catalyst loading in a photoreactor and the total reaction rate, up to a certain limit. This limit corresponds to the maximum amount of photocatalyst one can have in the reactor, in which the entire surface of the particles are fully illuminated. For higher quantities of catalyst in the reactor, the particles would be in excess and mask part of each other surfaces from the light. For an optimal and efficient photoreforming reaction, the catalyst mass should be kept at this point or below, while the photon flux should be kept in the first regime for maximum energy efficiency. The reaction rate's dependence on the discussed parameter are summarized in figure 6 below.

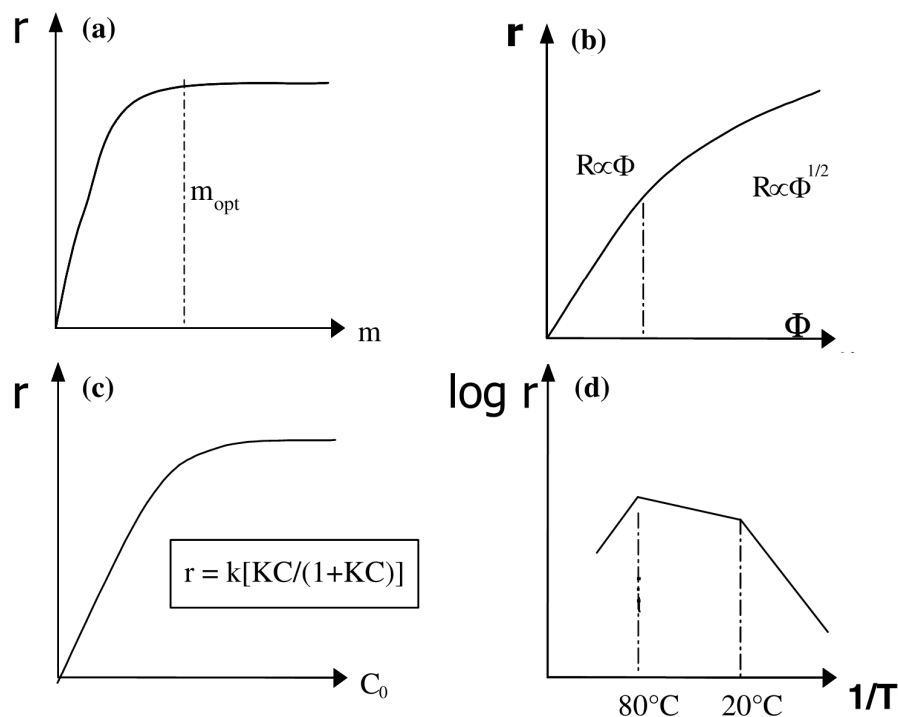


Figure 6: The figure illustrates the reaction rate's dependence on:(a) mass of catalyst, (b) radiant flux, (c) initial substrate concentration and (d) temperature [18].

One final parameter that affects the reaction rate is the nature of the sacrificial agent. Bahruji *et al.* conducted experiments with several different substrates on a Pd–TiO₂ catalyst in order to compare their activity in a photoreforming reaction and to attempt to find a pattern or explanation as to why some substrates are active and some are not. They found that the photocatalytic reforming process requires a substrate having an oxy-function with at least one α -hydrogen atom in order to produce detectable amounts of hydrogen [19]. The activity of the different substrates are plotted together in figure 7 below:

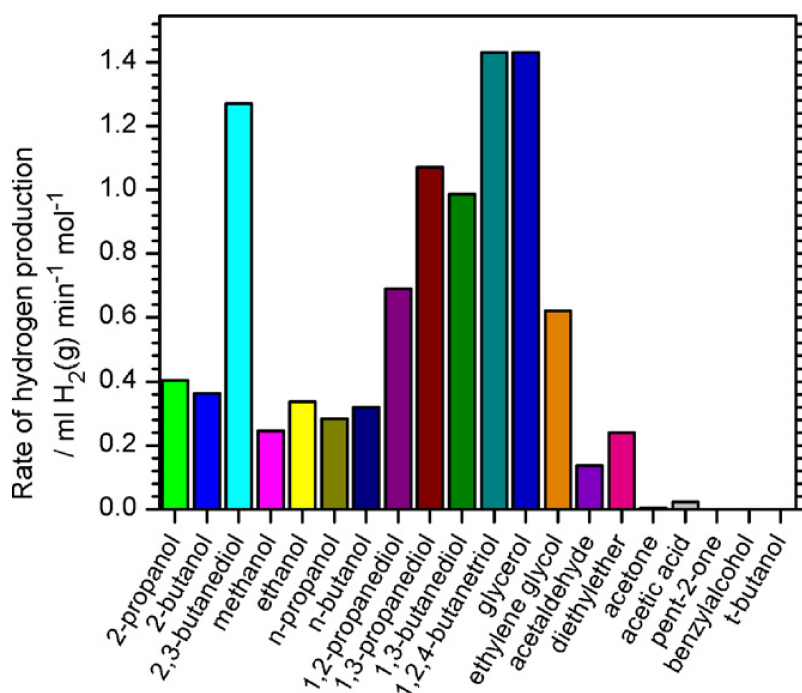


Figure 7: The figure shows a comparison of the activity of different sacrificial agents a photoreforming reaction over a Pd–TiO₂ photocatalyst. [19]

It is important to note that this preference of substrates is unique to the Pd–TiO₂ photocatalyst, which means that a Cu–TiO₂ photocatalyst could yield different results during a similar experiment.

2.5 Commercial applications of TiO₂ photocatalysis today

Titania's usage is not limited to only photocatalysts, the material possesses several unique properties which makes it useful in a wide range of applications. Figure 8 below shows a summary of the most important applications of TiO₂ [14].

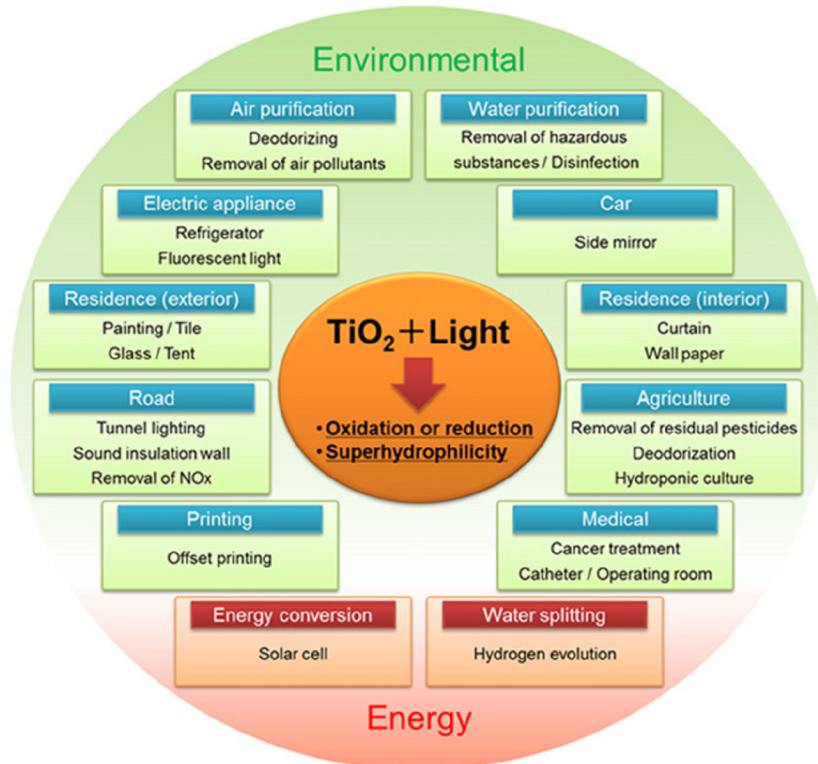


Figure 8: The figure shows a summary of the different applications for the photocatalytic material TiO₂.

Titanium oxide possesses a really rare property: It changes its hydrophilic nature when irradiated with UV photons. The contact angle of water on TiO₂ decreases gradually over time if the material is exposed to UV light, reaching almost 0°. This causes water on the surface to form a thin film instead of drops, which keeps the surface transparent and resistant to fogging. This is taken advantage of by coating mirrors and glass with TiO₂ to preserve the transparency under wet conditions during daytime

. Picture 9 below shows an example of this [20]

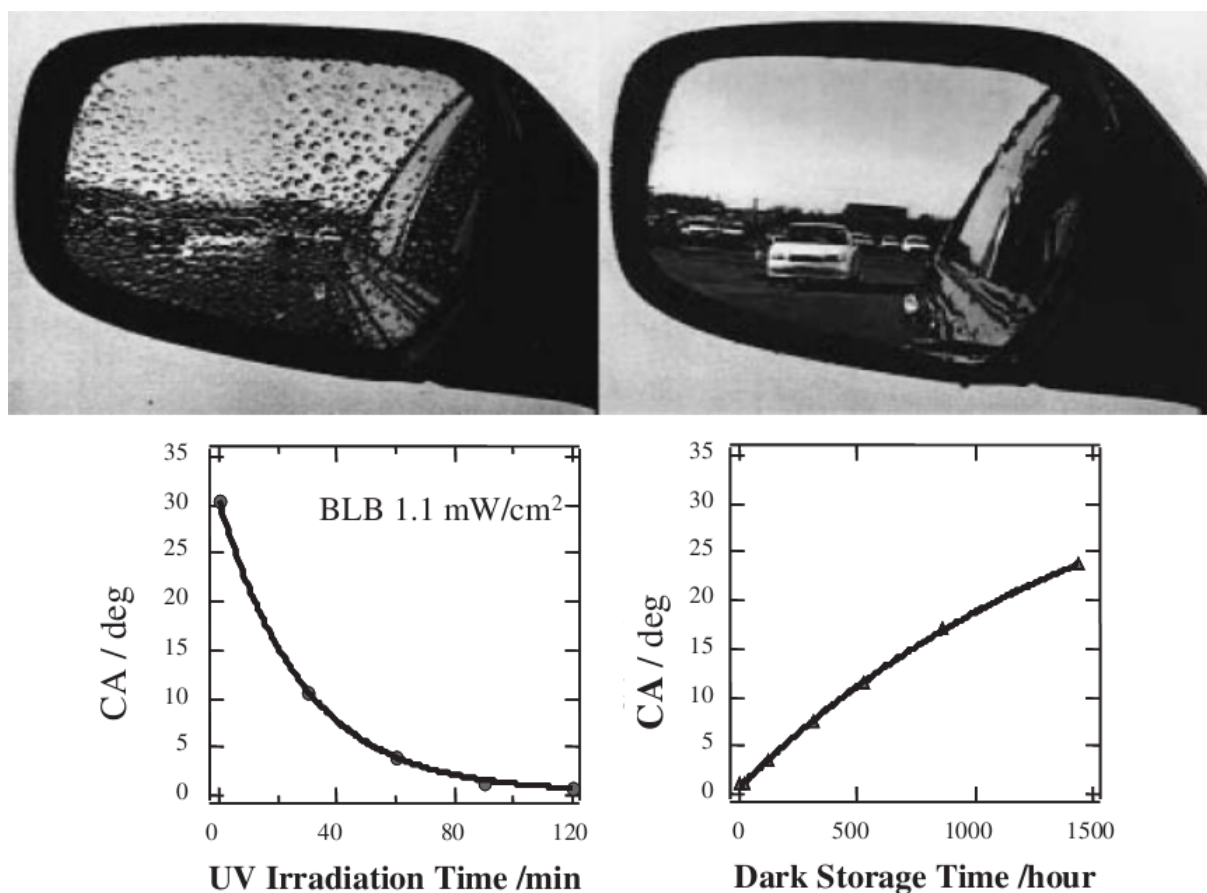


Figure 9: The picture shows the effect of TiO₂ when coated on an automobile side-view mirror (right) compared to a traditional mirror (left). The graphs below the picture shows how the presence and absence of light affects the contact angle of water on the TiO₂ surface over time.

A downside with this technology is the fact that it's not very effective in areas where the sunlight is weak, like on the northern hemisphere during the winter. It can however be used to some extent indoors, like in anti-fogging mirrors in the bathroom where there is a low but sufficient radiation density of UV rays. Another interesting property of TiO₂ is the antibacterial effect it exhibits when exposed to UV rays. This effect alone is too weak to be useful indoor, but by depositing copper on the surface the effect becomes strong enough even when only exposed to weak UV-light. It is believed that TiO₂ assists the intrusion of copper ions into the bacterial cells, which ultimately kills them. Photocatalytic tiles which kills bacterias are available today and they even reduce the number of bacterias in the air around them. [14]

Surfaces coated with TiO₂ will also oxidise organic molecules to CO₂ when exposed to UV rays. This effect is used to make self cleansing surfaces, where dirt is removed "photocatalytically". The same principle is used to clean the air from VOCs (volatile organic compounds) and to purify water [21]. Some Japanese highways have street lights

covered with TiO_2 containing glass, which keeps them clean from exhaust particles and dust. Titanium oxide has also been coated on a 500 m long road stretch near Osaka in Japan, where it oxidises NO_x gasses to NO_3^- ions that are washed away by the rain and thus making the air cleaner [13]. Photocatalytic water splitting and photoreforming are possible to perform in a lab, but the efficiency is still too low to be of any commercial interest [21].

2.6 General properties of TiO_2 and modifications

Titanium dioxide is a white coloured semiconductor that exists as three different polymorphs; anatase, rutile and brookite [22]. The most stable form is rutile, which is the main source of TiO_2 . All of the three polymorphs are possible to synthesize in the laboratory but the metastable brookite and anatase will transform to the thermodynamically stable rutile when calcined at temperatures exceeding $600\text{ }^\circ\text{C}$ [23]. What all three forms has in common, is the fact that Ti^{4+} atoms are co-ordinated to six O^{2-} atoms forming TiO_6 octahedra [24]. The figure below shows the structural differences in detail.

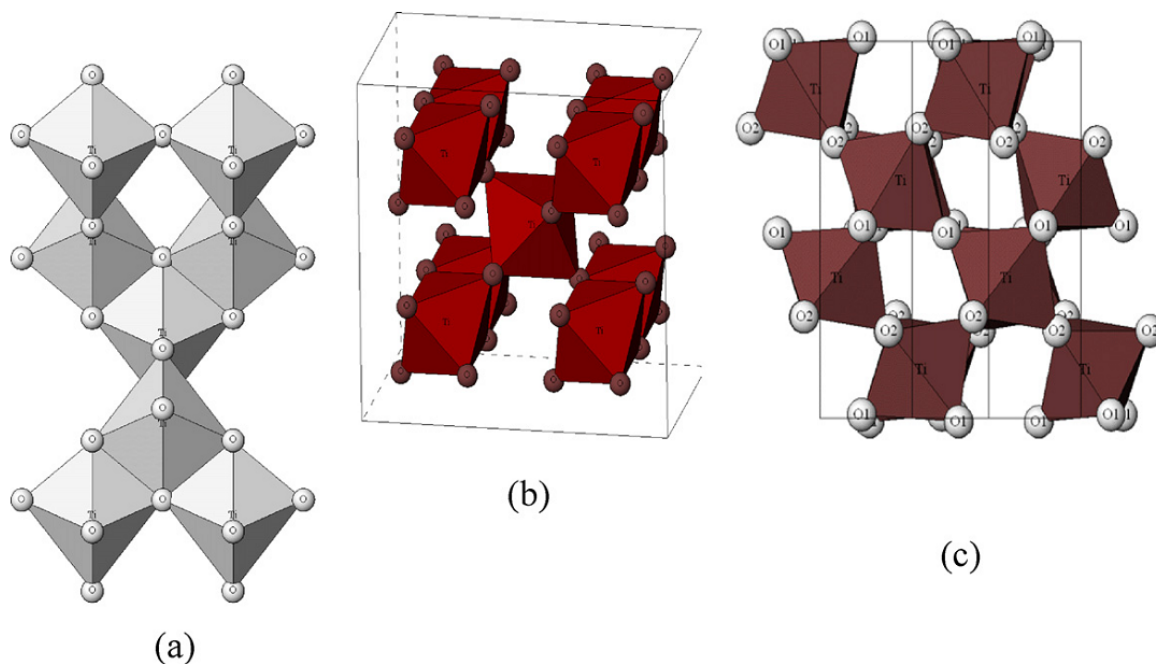


Figure 10: The figure shows the three polymorphs of TiO_2 : anatase (a), rutile (b) and brookite (c) [25].

The bandgaps of the different polymorphs are somewhat similar but there is a minor but significant difference. The bandgaps are 3.2 eV for anatase and brookite, but for rutile the bandgap is 3.0 eV [25]. The energy of these bandgaps corresponds to the energy of UV-light at a wavelength shorter than 380 nm. This is the reason for titania's poor photocatalytic performance when irradiated with sunlight, which as already mentioned only contains about 5 % UV-rays. Because of oxygen deficiency TiO_2 is typically an

n-type semiconductor [26]. Today TiO_2 is by far the most investigated photocatalyst, and this is due to low cost, high photo-activity and resistance to photocorrosion, low toxicity and good chemical and thermal stability ([25], [27], [28], [29]). The toxicity is practically absent, which is why it's even used in food additives, toothpaste and as an UV-blocker in sunscreens [30] [31]. In this project a type of commercial TiO_2 called "Degussa P25" was used. P25 contains around 80% anatase and 20% rutile [25] with a moderately high surface area of about $50 \frac{\text{m}^2}{\text{g}}$ and a particle size of 25 nm [32]. Pure anatase is the most active polymorph of TiO_2 , but when in physical contact with rutile the activity is even higher. This can be explained by looking at the conduction band of rutile which is slightly more positive than that of anatase. This causes rutile to act as an electron sink for anatase which inhibits recombination. This is illustrated in figure 11 below.

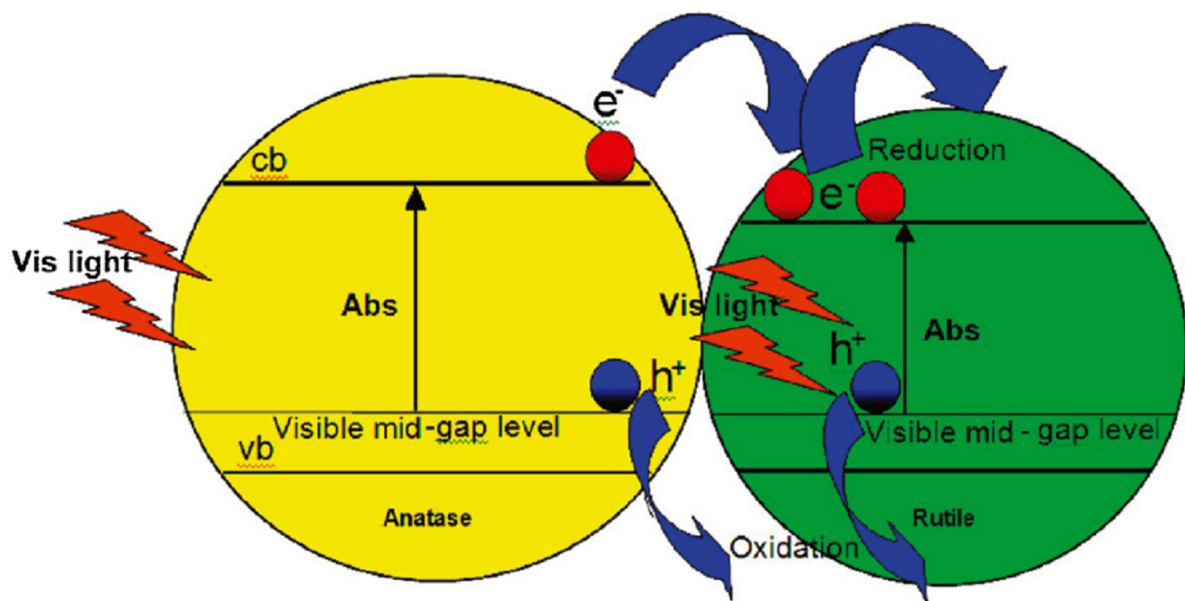


Figure 11: The figure shows the effect of combining anatase and rutile [25].

A very similar effect is achieved when noble metals like Pd, Pt and Au are deposited on titania. The excited electrons migrate to the noble metal until the two Fermi levels are aligned, where they avoid being recombined with the holes. The electrons are kept in the noble metals by a Schottky-barrier which is formed on the interface between the noble metal and TiO_2 , until they are consumed by H^+ . The hydrogen production rate is reported to greatly increase when noble metals are used as a co-catalyst, where Pt seems to be the most effective metal [6].

2.6.1 Strategies for improving titania's photoactivity

The largest drawback of TiO_2 as a photocatalyst is the fact that it may only utilize up to 5 % of the incoming sunlight because of its high bandgap. Numerous attempts have been made to extend the adsorption spectrum of TiO_2 into the visible light region by reducing this bandgap. In figure 12 below, one can see how much the harvesting of sunlight could be increased by lowering the bandgap.

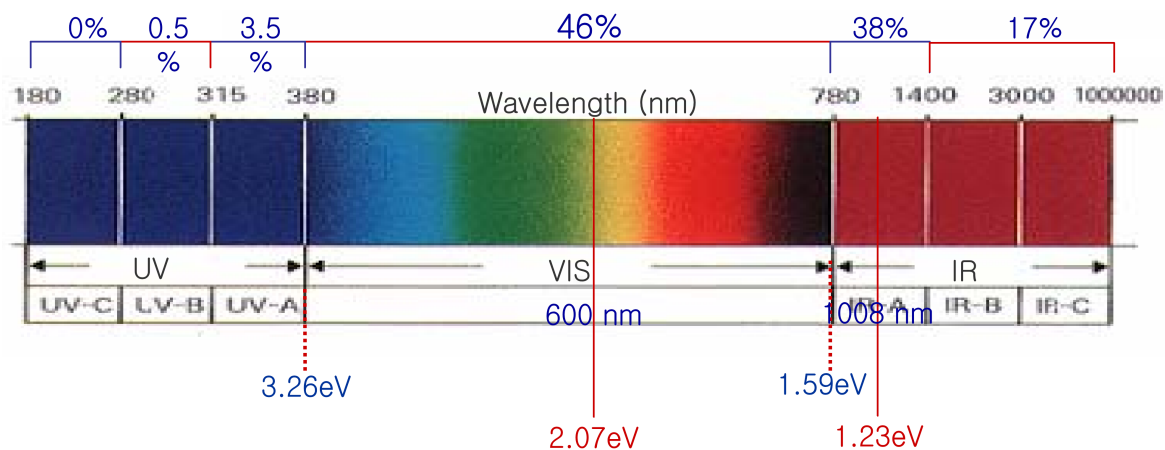


Figure 12: The figure shows the motivation behind narrowing the bandgap of TiO_2 , which is to harvest more sunlight [33].

Titania has been doped with transition metals such as Cr, V, Co and Fe which successfully decreased the bandgap and increased the photocatalytic activity [25] of the material. The idea is that the incorporation of transition metals into the crystal lattice of titania may result in the formation of new energy levels between the valence band and the conduction band. This would induce a shift in the adsorption towards the visible light region. The drawback of this approach is that the transition metals may also act as recombination sites, decreasing the quantum efficiency of the catalyst by increasing the rate of recombination [25]. The same has been done with some p-block elements such as N, C, B, and F where very similar effects were observed. So far it seems that co-doping titania with both N and B gives the best results [34].

Fortunately, doping is not the only way to narrow titania's bandgap. The research group of Matthias Batzill tried a new approach where they performed a study of the rutile (011) surface. They discovered that after cleaning the rutile (011) surface by argon ion irradiation before annealing the sample in a low pressure of oxygen, the surface atoms had re-arranged themselves into a hexagonal pattern. Photoemission spectra was used to determine the bandgap of this two-dimensional phase which was found to be about 2.1 eV, meaning that visible light up to 590 nm could be adsorbed. It still remains to find out if this new surface phase may be created on smaller crystals and if the catalyst will perform satisfactory over time in realistic photocatalytic conditions. [35]

A research group lead by Samuel Mao also took a different approach to narrowing the bandgap of TiO_2 . They managed to reduce TiO_2 in a hydrogen atmosphere which made the material turn black, a good sign when the goal is to make the TiO_2 adsorb as much light as possible. This treatment narrowed the bandgap down to incredible 1 eV which corresponds to light up to 1200 nm. This material was loaded with 0.6 wt.% Pt and the catalyst was tested under irradiation from a sunlight-simulating lamp where it yielded a promising $10 \text{ mmol H}_2 \text{ h}^{-1} \text{ g}_{\text{cat.}}^{-1}$. This was a persistent production rate and the catalyst was tested for several days without much sign of deactivation. It was calculated that 24% of the incoming sunlight was harvested to produce H_2 gas, which is a very high efficiency for TiO_2 [35] [36]. As a comparison, the experiments in this project yielded a quantum efficiency of only 0.41 % with UV radiation on copper loaded P25 titania.

Nano-structuring of TiO_2 is another subject that has received much attention during the recent years. The motivation behind performing nano-structuring of TiO_2 can be to increase the overall surface area of the catalyst, to shorten the diffusion paths of the reactants and to avoid recombination of the electron and the hole in the bulk phase. All of these effects should contribute to increasing the activity of the photocatalytic TiO_2 material. The rate of recombination in the bulk phase is reduced by decreasing the size of particles so the surface to volume ratio is favorable, and by making sure the particles have a high degree of crystallinity which minimizes the number of bulk defects acting as recombination centers [25]. In addition to usage photocatalysis, titania-based nanomaterials also show promising potential applications in gas sensing devices and solar cells. The nano-structures are systematically classified into different groups depending on their geometric shape.

The zero-dimensional group consists of spheres which can be either filled with bulk material or be more or less hollow. These particles usually possess a high specific surface area, they have a high pore volume and high pore size. These attributes result in high photocatalytic activity because of the high amount of accessible surface and good conditions for mass transfer. Enhanced light-harvesting is also a factor which helps on the photocatalytic activity and occurs because light is allowed to access not only the external surface area but also the internal surface area of the hollowed sphere [14].

The one-dimensional group consists of fibers and tubes that have most of the same advantages as the zero-dimensional group, except for the enhanced light harvesting. Titania fibers are already used in other applications like gas sensing and batteries [14]. The two-dimensional group consists of TiO_2 nanosheets which is a very thin, flake-shaped material with a high aspect ratio. This material has low turbidity, high smoothness and excellent adhesion to substrates which make it well suited for self-cleaning coatings. Like normal titania, this nano-coating will also become superhydrophilic when exposed to UV-light. This is the reason for its usage on car mirrors and non-fogging goggles as shown in figure 9 on page 16.

The last group is the three dimensional group, in which we find the interconnected TiO_2 architecture. This structure has potential applications in steady-state photo reactors as a TiO_2 sponge may be produced and used instead of TiO_2 powder. While the total

surface area may suffer, usage of the TiO_2 sponge has the advantage of not requiring a separation step as there is no catalyst powder that has to be separated from the outgoing liquid. This gives it a practical advantage over traditional powder based TiO_2 because filtering of outgoing flow can be omitted [35]. Figure 13 below shows a summary of the different nanostructures along with their key properties.

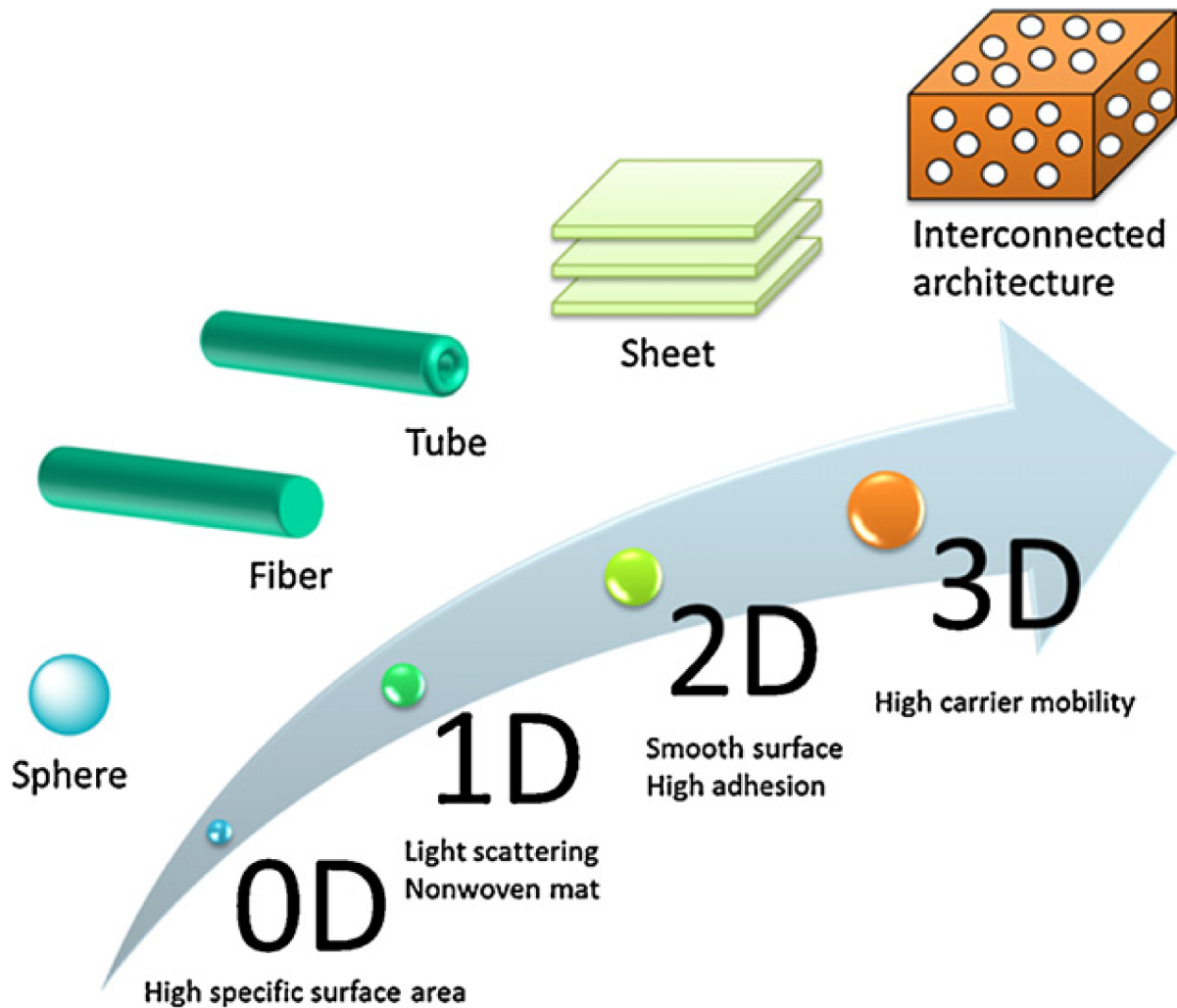


Figure 13: The figure shows some different nano structures of titania [25].

2.6.2 TiO₂ loaded with copper and other co-catalysts

In photoreforming, the activity of pure TiO₂ is usually negligible in the absence a co-catalyst. The previous subsection discussed ways to improve the titania part of the photocatalyst, while this subsection focuses on the co-catalyst part. Noble metals such as platinum, palladium, rhodium, gold and ruthenium will greatly enhance the photocatalytic activity of TiO₂ even with loadings as low as only 1 wt.% [6]. In the recent years, great emphasis has been put on replacing these expensive noble metals with more common metals without sacrificing too much of the photocatalytic activity. This would dramatically reduce the cost of the photocatalyst making the process more economically viable. Judging from recent scientific papers, it seems like copper is a very good alternative to noble metals as a co-catalyst. The photoactivity is decent and the stability is good. The copper is usually present as CuO and Cu₂O which are the most active, and some of it may even be present as metallic copper which also has a lower but significant activity [3]. Even though copper usually exists in oxide form, it will be referred to as "copper" or "Cu" for simplicity.

Xu and Zhang [3] has reported an achieved hydrogen generation rate of 9-20 mmol h⁻¹ g_{cat.}⁻¹ depending on the fabrication method. Sreethawong and Yoshikawa [37] reported that in comparison to Pt, Au, and Pd metals, Cu showed only slightly weaker enhancement of TiO₂ activity for hydrogen generation. The reported optimal copper loading is ranging from 1.2 wt% to 8.12 wt% in the articles that have been studied. Below is a summary-table of several studies where the optimal copper loading for TiO₂ is listed, along with the corresponding hydrogen evolution rate and fabrication method. The fabrication methods will be explained in detail later in this section, starting on page 28.

Table 1: The table shows a summary of results from different experiments.

Optimal copper loading [wt.%]	Fabrication method	Additional details	H ₂ evolution $\left[\frac{mmol}{hgcat}\right]$	Reference
6.97	DP	10 vol% methanol	20	Xu <i>et al.</i> [3]
6.55	Sol-gel	10 vol% methanol	15.5	Xu <i>et al.</i> [3]
1.2	Sol-gel	42 vol% methanol	3.0	Wu <i>et al.</i> [38]
1.5	Single step sol-gel		0.36	Yoshikawa <i>et al.</i> [37]
8.12	Impregnation	50 vol% methanol	13.5	Choi <i>et al.</i> [39]
1.3	Impregnation	0.1 M glycerol	2.06	Yu <i>et al.</i> [40]
7.38	impregnation	10 vol% methanol	18.5	Xu <i>et al.</i> [41]
7.0	Impregnation	5 vol% methanol	0.82	Bandara <i>et al.</i> [42]

It is important to note that this is only a rough comparison intended to give the reader a feeling of what has been done in the field of Cu–TiO₂ photocatalysis. The experimental conditions were not the same, as different substrates and substrate concentrations have been used along with different photoreactors and light intensities. The catalyst loading during the experiment is also a major factor in deciding specific activity, as the Results and Discussion section later will elucidate (section 4.1.1). In addition to this, it is not always clear whether the reported copper content is based on copper being in metallic or in oxide form.

Some important information which can be extracted from this comparison is the fact that increasing the copper content beyond 8 wt.% is unnecessary as this will cause the activity to decrease. Experiments have been conducted which proves that pure CuO, pure CuO₂ and pure TiO₂ barely generates any hydrogen at all, while TiO₂ loaded with optimum Cu content is highly active in comparison. From what is known so far, it seems that the reaction sites for hydrogen generation is likely to be at the periphery of Cu_xO on TiO₂. If the copper content is increased beyond the optimum loading, the metal particles will start to merge together leading to a shrinking periphery. It is also likely that copper species will block some of the light that needs to be adsorbed onto the TiO₂ and thus decreasing the density of incoming photons leading to decreased photocatalytic activity [43].

As mentioned earlier, Sreethawong and Yoshikawa compared Cu to Pd and Au as a co-catalyst for TiO₂. The results are illustrated figure 14.

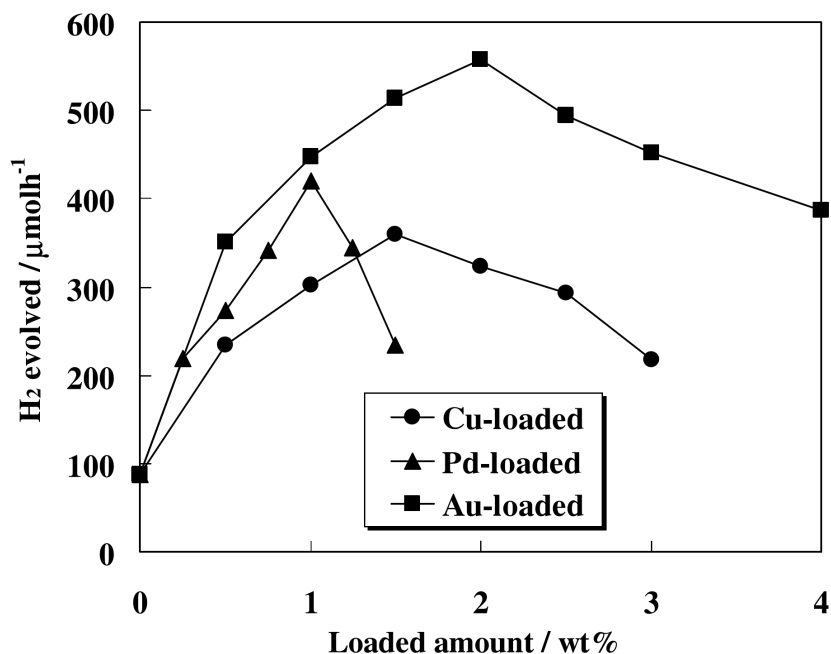


Figure 14: The figure shows copper is only slightly less active than the precious metals as a co-catalyst for TiO₂ [37].

An important difference to remember between copper and the other precious metals is the fact that copper will be mostly in oxide form when deposited on TiO₂. This depends of course on the preparation method, but when Cu(NO₃)₂ · 3H₂O is calcined in air it will decompose and form copper oxides (Cu_xO) which are semiconductors. This is explained more in detail at page 28. Even though the Cu_xO semiconductors are deposited on titania instead of a metal in its metallic state which usually is the case, the semiconductor co-catalyst successfully acts as an electron trap because the conduction bands of both copper oxides are lower than the conduction band of TiO₂. This causes electrons to migrate from the titania to the copper oxides, preventing recombination and causing Cu_xO to act as reduction sites.

This electron transfer is illustrated in figure 15 below.

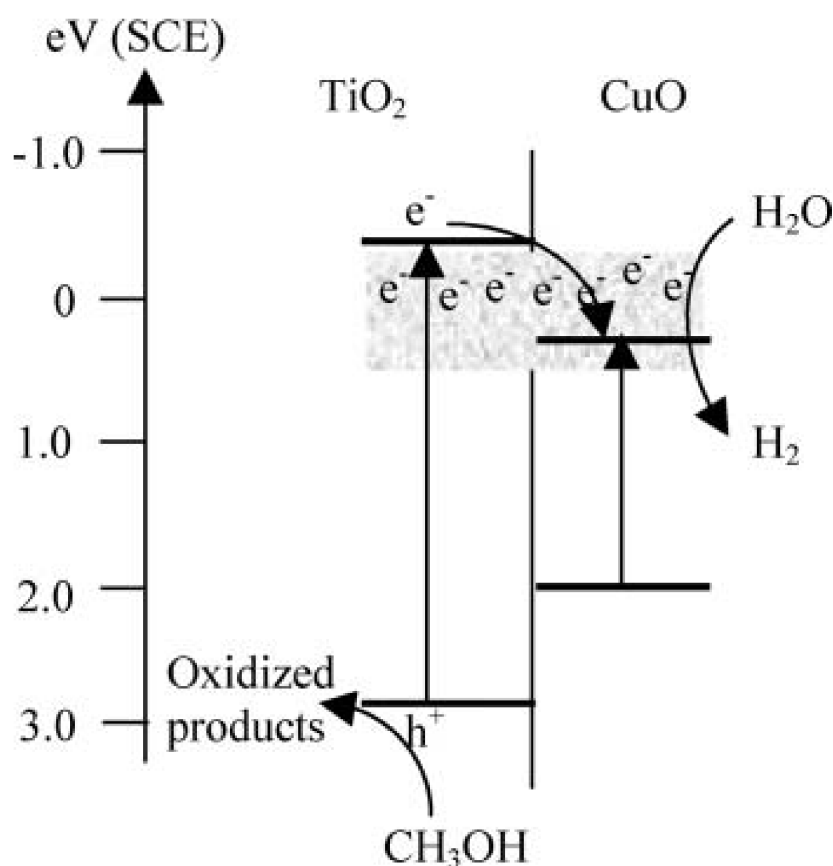


Figure 15: The figure shows how CuO act as an electron trap for TiO₂ [42].

Xu and Zhang [3] performed a systematic study to find out which fabrication method yielded the most active Cu–TiO₂ photocatalyst with respect to hydrogen evolution rate. They tested out four methods: In situ sol–gel (SG), incipient wetness impregnation (IWI), deposition precipitation (DP) and in-situ photo-deposition (PD). They discovered that the method of fabrication affected the chemical state of Cu, the distribution of Cu within the catalyst, BET surface area and even the crystal structure of the TiO₂. The DP method lead to the highest initial hydrogen evolution rate, while the SG method achieved the highest hydrogen evolution rate over time because of its excellent stability. This stability is likely to come from the resistance to Cu leaching because of its crystal configuration. The method yielding the least active photocatalyst was the PD method. The authors conclude that the chemical state of copper is closely related to the activity of the catalysts, where the Cu₂O is slightly more active than CuO while both of these oxides are superior to metallic copper. The reason for this is the fact that the redox potential of Cu⁺/Cu (0.52 V) is higher than Cu²⁺/Cu (0.34 V) which makes the electrons preferentially migrate to Cu₂O [3].

When nanostructured titania is combined with a fitting co-catalyst, the result may be an excellent photocatalyst which is specifically tailored for photocatalytic hydrogen production. Xu *et al.* combined TiO_2 nanotubes with CuO and achieved an incredible H_2 evolution of $71.6 \text{ mmol h}^{-1} \text{ g}_{\text{cat.}}^{-1}$ [3]. A final trick that deserves to be mentioned is "dye sensitizing". Dye-sensitization is already widely applied in solar cells and it also works to some degree in photocatalysis where it can extend the photoresponse of TiO_2 into the visible region. The principle is that the incoming photons are absorbed by a dye instead of the TiO_2 phase where it excites an electron from the highest occupied molecular orbital (HOMO) to the lowest unoccupied molecular orbital (LUMO) of the dye. The dye's LUMO has higher energy than the conduction band (CB) of TiO_2 causing the electrons to be transferred to the CB of TiO_2 where they can migrate to the co-catalyst (if present) and reduce H^+ to H_2 or O_2 to $\text{O}_2^{\bullet-}$. The dye on the other hand, is converted to its cationic radical which is why an additional red-ox couple is needed, in order to bring the dye back into its original electronic state by reducing either water or a sacrificial agent like methanol [6] [25]. The mechanism is illustrated in figure 16 below.

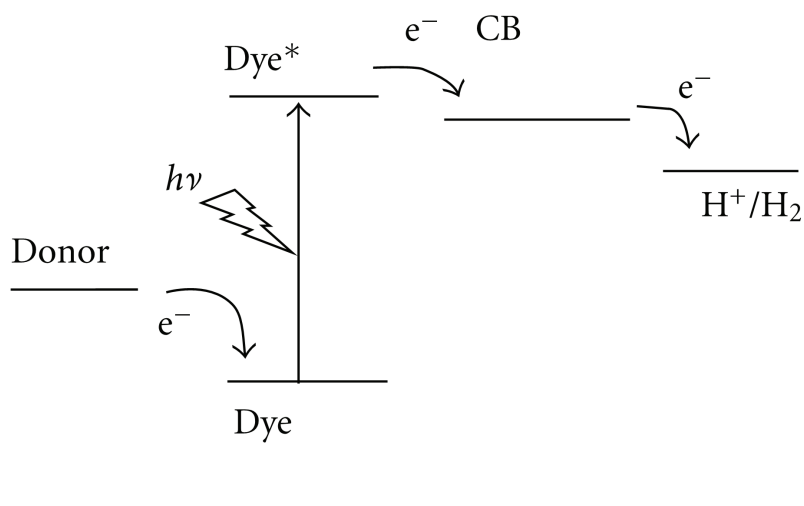


Figure 16: The figure illustrates the mechanism of dye sensitization [25].

2.7 Alternatives to titania

Titanium oxide is not the only viable semiconductor for photoreforming and water splitting. In 2008, almost 25 % of the published articles related to photocatalysis described studies on substitute materials to TiO_2 . Among these were mixed oxides of transition metals like V, Nb and Ta, usually containing some main group elements such as Bi, Sb, In or Ga. These materials along with sulfides and nitrides of different metals have been studied extensively in hope to obtain materials with decent photoactivity in the visible range. [44]. When it comes to photoreforming with methanol, some niobates with the general formula $AB_{n-1}Nb_nO_{3n+1}$ where A=K, Rb, and Cs while B= Ca, Na, Sr, or Pb and n= 3-4 have shown a remarkable photoactivity for H_2 production. As an example, $\text{HCa}_2\text{Nb}_3\text{O}_{10}$ with Pt as a co-catalyst produces as much as $19 \text{ mmol H h}^{-1} \text{ g}_{\text{cat.}}^{-1}$ [44].

Because the liquid phase during a photoreforming reaction is less oxidising than during photocatalytic water splitting, sulfide semiconductors can withstand the process and thus be used in photoreforming without suffering too much from photo-corrosion. This is the main reason for materials like ZnS and CdS to receive renewed attention, and the latter is reported to perform remarkable on its own and even better when combined with materials like Ag_2S , ZnS or CdO as long Pt or Ru co-catalyst is present. In the year 2009, nanostructured CdS (in the form of nanosheets or hollow nanorods) held the record for photoactivity at 440 nm visible light with a quantum efficiency of 60 %.

A very important parameter for the photocatalytic materials are the band positions. As already mentioned in section 2.3, the redox potential of the conduction band needs to be more negative (higher in energy) than the acceptor molecule (H^+) so that a reduction may take place. When it comes to the position of the valence band, the requirement is less strict if the photocatalyst is to be used in photoreforming rather than water splitting. In the water splitting, the position of the valence band need to be more positive than the redox potential of oxidised molecule which is H_2O at 1.23 V. In photoreforming on the other hand, the oxidation of methanol requires a potential of only 0.7 V which in theory opens up the possibility for more semiconductors to be used.

This is shown in figure 17 below.

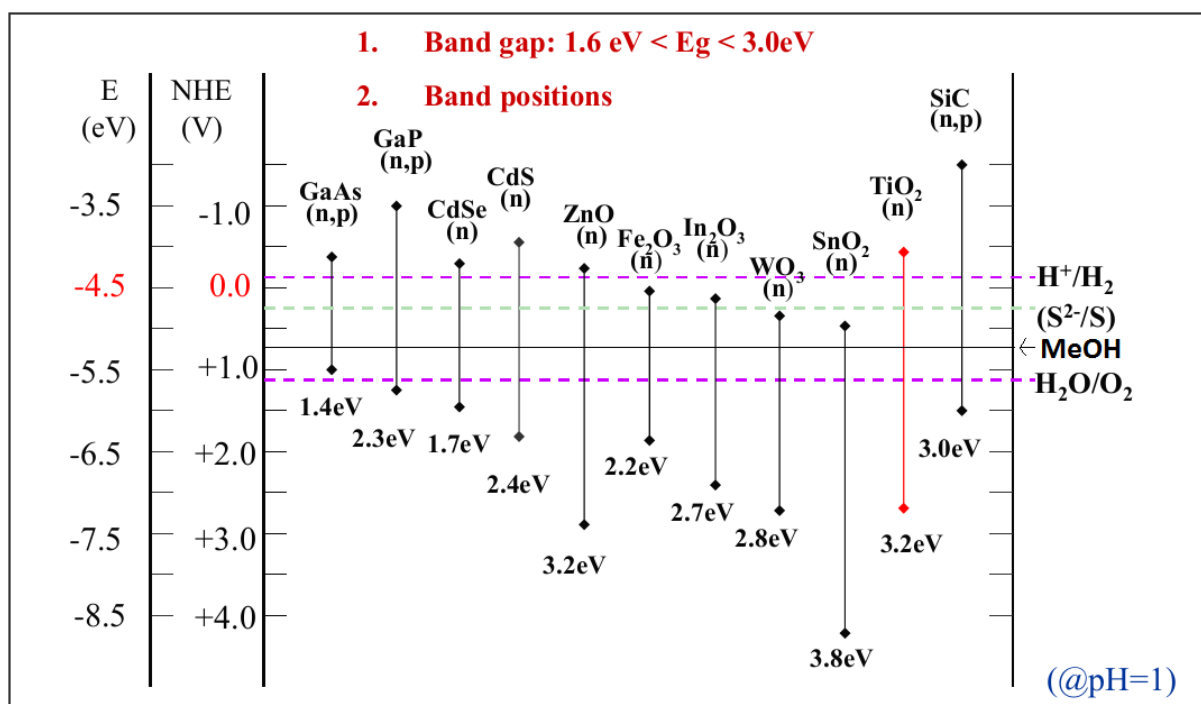


Figure 17: This figure shows the band position of some common semiconductors.

Note how GaAs could in theory be used in photoreforming but not in photocatalytic water splitting. The list of alternative materials to TiO₂ could go on for several pages, so this sub chapter will end with some honorable mentions. In 2009 the record holding photocatalyst for water splitting was a $(\text{Ga}_{0.88}\text{Zn}_{0.12})(\text{N}_{0.88}\text{O}_{0.12})$ semiconductor combined with $\text{Rh}_{2-x}\text{Cr}_x\text{O}_3$ as a co-catalyst which achieved a quantum yield of 5.9 % at 420-440 nm. Some other water-splitting catalysts are La doped NaTaO₃ [45], Sr₂Nb₂O₇ [46], Sr₂Ta₂O₇ [46], La₂Ti₂O₇ [47], K₂La₂Ti₃O₁₀ [48], NaTaO₃-NiO [6]. They all share a critical drawback with TiO₂ though, which is the fact that they require UV light to be active, limiting solar light harvesting. Some great photocatalysts for photoreforming are SrTiO₃ nanocrystals and thiourea-doped Na₂TiSi₅O₁₁ zeolite [6]. In South Korea, scientists from Pohan University have created a photocatalytic system using partly oxidized wolfram on a $\text{PbBi}_2\text{Nb}_{1.9}\text{Ti}_{0.1}\text{O}_9$ which shows promising activity in photoreforming reactions [33].

2.8 Fabrication methods of TiO₂ based photocatalysts

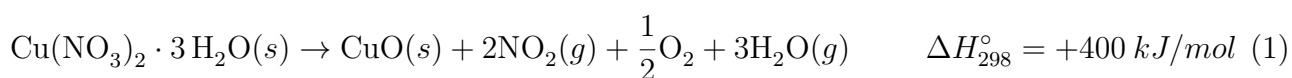
As already mentioned, the performance of photocatalysts is related to the method of fabrication. Particle size, chemical state of Cu, distribution of Cu, BET surface area and crystal structure are parameters that depend on the fabrication method. In this section, the most common methods will be briefly explained.

2.8.1 Incipient wetness impregnation (IWI)

This method is also called dry impregnation or capillary impregnation. The active metal precursor is dissolved in an aqueous or organic solution before the catalyst support is added. The volume of the solution should be equal to the pore volume of the catalyst support, and the solution is drawn into the pores by capillary action. In this particular project the metal precursor is Cu(NO₃)₂ · 3 H₂O and TiO₂ is referred to as the support even though it participates in the photoreaction. The maximum metal loading which is possible to achieve by this method, is limited by the solubility of the metal precursor in the solution [49]. After the impregnation is done, the sample is dried to get rid of humidity and volatile compounds. After drying, the sample is calcined where the metal precursor is converted to the pure metal or to a metal-oxide. An interesting trait about this method is that the CuO will be deposited to a high degree inside the TiO₂ pores rather than on the surface [50].

2.8.2 Calcination

Calcination is defined as "The process of heating a substance to a high temperature but below the melting or fusing point, causing loss of moisture, reduction or oxidation, and dissociation into simpler substances" [51]. Calcination is thermal treatment of the catalyst which is often performed under atmospheric conditions. This treatment will usually decompose metal precursors into its oxide form, but it may also reduce noble metals to their metallic form if performed in hydrogen flow at sufficiently high temperatures. In this project calcination was performed on TiO₂ impregnated with Cu(NO₃)₂ · 3 H₂O for 4 hours at 200 °C, which caused reaction 1 to happen:



For higher temperatures, some Cu₂O can also be formed. The ratio of CuO to Cu₂O depends on the calcination temperature and time, but for the reduction of CuO (Cu²⁺) to Cu₂O (Cu⁺) to be spontaneous the temperature has to exceed 950 K which is rarely the case (see Appendix A for calculation). This suggests that for all practical purposes, the copper species deposited on titania after calcination is only CuO. The reason it is sometimes referred as Cu_xO, is because partial reduction of the copper species takes place during the photoreforming reaction [3]. When the calcination process is completed, the active metal or metal-oxide is deposited on the support and the catalyst is usually ready for use.

2.8.3 Deposition precipitation method

In this method the metal is precipitated on the support by conversion from a soluble precursor. This conversion can be achieved by changing the pH of the solution, by changing the concentration of a complexing agent or through redox reactions changing the valence state of the metal. This method is usually demanding compared to other alternatives, but it is still one of the most frequently used methods. This is because the method has the strength of producing materials of high purity and the process can easily be tailored to produce a product of desired quality [52]. This method can also be applied to produce a Cu–TiO₂ catalyst. This is done by mixing Cu(NO₃) and P25 in an ice bath water batch and adding NaBH₄ as a reducing agent. After 2 hours of vigorous stirring the copper ions are reduced to Cu₂O and precipitated on the P25 support. According to Xu *et al.* this is the method that yields the most active copper based TiO₂ catalysts because Cu₂O is the most active copper compound compared to CuO and metallic Cu [3]. This method also tend to deposit a relative large percentage of the particles on the surface of the support, rather than in the pores [50].

2.8.4 Photo deposition method

This method is by far the easiest and fastest way to produce TiO₂ based catalysts, but the success of the method depends strongly on the metal of choice. The metal pre-cursor is dissolved in a mixture of methanol and water together with P25 TiO₂ or a similar titania source. The mixture is sonicated and UV radiation is applied for a few hours. Methanol acts as a reducing agent, reducing metal ions from the precursor to it's metallic form which is deposited on the titania. In other words, the metal is deposited on the support while the photoreforming experiment is running. This method works well with gold but is less successful with copper, because metallic copper is deposited instead of the more active copper oxides [3].

2.8.5 Sol-gel method

The sol-gel process can be described as "Formation of an oxide network through polycondensation reactions of a molecular precursor in a liquid." [53]. A sol is a stable suspension of colloidal particles or polymers in a solvent, meaning that the particles are so small (1 nm-1 μm) that they are pretty much unaffected by gravitational forces. A gel consists of a three-dimensional continuous network, which is surrounded by a liquid phase. In a colloidal gel, this network is built from colloidal particles that have agglomerated, forming continuous branched chains consisting of very small particles that stick together due to van der Waals and electrostatic forces.

The process is illustrated in picture 18 below.

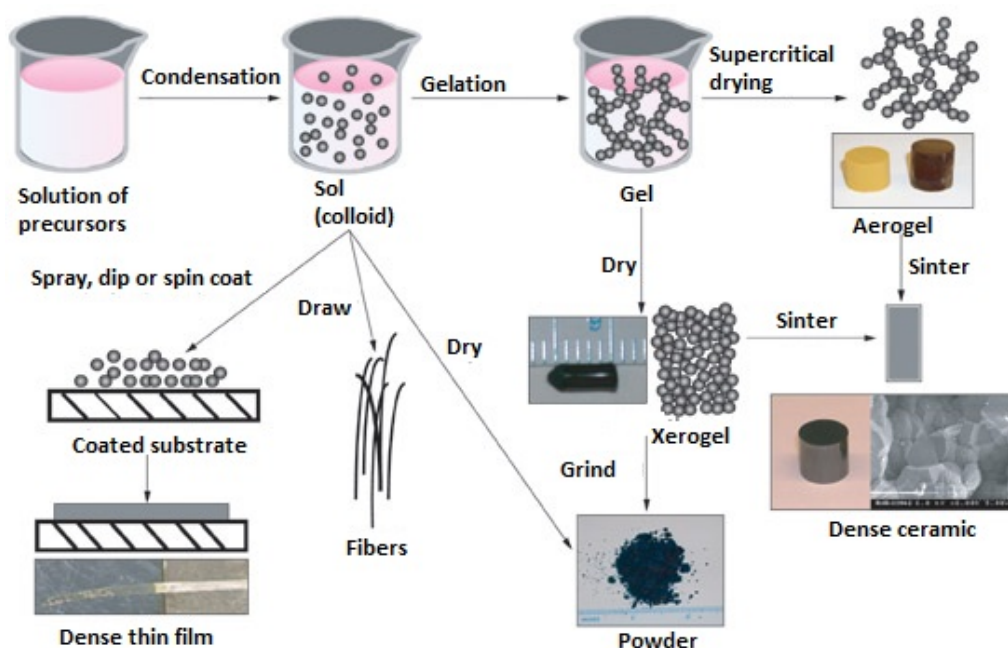
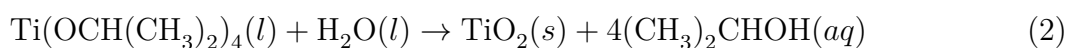


Figure 18: These are the different steps involved in a sol-gel synthesis [54].

The sol itself is made by hydrolysis and partial condensation of a precursor, usually a highly reactive alkoxide or an organic epoxide [54]. The gel is formed when the formed particles aggregate. Nanoparticles of TiO_2 can be made by this method, where the Ti precursor is Titanium isopropoxide with the chemical formula $\text{Ti}(\text{OCH}(\text{CH}_3)_2)_4$. This compound will undergo hydrolysis in contact with water according to reaction 2 below [55].



After the TiO_2 gel is formed, it is dried into a Xerogel (see fig.18) and grinded to form a powder. The advantages of this method is that the synthesis is easily controlled and several parameters may be changed in order to optimize the product. The TiO_2 particles synthesized by this method are generally smaller than the commercial P25 TiO_2 , leading to a larger surface area. As an example, Xu *et al.* has reported a particle size of 8.5 nm by the sol-gel method while the P25 particle size was measured to be about 25 nm [3]. In the same study, the catalyst made by the sol-gel method achieved the best stability over time because some Cu was likely to be incorporated in the TiO_2 lattice which prevents the loss of copper through leaching.

2.9 Deactivation in photoreforming and water splitting

Even though photocatalytic water splitting and photoreforming are mostly performed in aqueous phase at ambient temperatures, the problem of deactivation is not entirely escaped. Semiconductors with sulfur anions like ZnS and CdS will oxidize over time and become inactive, especially if no sacrificial agents are present. Photocatalysts based on oxides like TiO₂ escape this problem but are vulnerable to others. An experiment was conducted by Xu *et al.* [3] where the concentration of copper ions were continuously measured during a photoreforming reaction using a Cu–TiO₂ photocatalyst. They found that the concentration of copper ions increases with time, which means that some copper is leaching into the solution from the catalyst. Copper is in principle stable at all pH values in pure de-ionized and de-oxygenated water, but during the photoreforming reaction in methanol a small part of it will still be dissolved over time. As already mentioned, the active sites of the Cu–TiO₂ are likely to be the interface of TiO₂ and the solid copper species, which means that the activity of the catalyst decreases if copper is removed from the solid phase. This holds true for catalysts where the copper content is at optimum or below, but it would be interesting to see how this deactivation mechanism affects catalysts having copper loading above the optimal. One could argue that copper leaching from these catalysts would further increase the activity, but this has yet to be confirmed. Xu *et al.* also found that Cu–TiO₂ catalysts fabricated by the sol-gel method were particularly resistant to copper leaching compared to other methods [3].

The most important source of deactivation during photoreforming is probably the accumulation of by-products. In a study by Xu *et al.* [41] The methanol-water solution was refreshed and this caused the photocatalyst to regain a substantial part of its activity. As time goes by, the methanol is slowly depleted from the solution when it is converted into H₂ gas. This converted methanol was refilled but it showed no effect on the hydrogen generation rate. Because replacement of the old solution showed much greater effect in regaining the photoactivity, it is likely that the main cause of deactivation is the accumulation of byproducts which inhibits the photoreforming reaction. According to Xu *et al.*, it is likely that one of these by-products is formic acid as the pH is observed to decrease with time as well [3].

Some other studies reports oxygen vacancies in the TiO₂ to be a major cause of deactivation, but this has yet to be confirmed in the case of photoreforming [56]. In literature there is a report by Wu *et al.* [38] linking decreased H₂ evolution to equilibrium, but this is pretty much disproved by the fact that refilling consumed methanol to the solution did nothing to increase the activity. The hydrogen gas generated is very limited and it escapes which keeps the system from ever reaching equilibrium. A study performed by Xu *et al.* revealed that reduction of CuO to metallic Cu could limit the electron transfer from TiO₂ and in this way deactivate the photocatalyst. In this study, the causes for deactivation was compared and their impact was ranked in following way: Accumulation of by-products (61.7 %), reduction of CuO (13.3 %), and copper leaching (6.7 %). There are still some unidentified factors, which hold 18.3 % of the total deactivation according to the author.

2.10 Surface area measurement by BET analysis

BET is short for Braun-Emmet and Tellersom, who are the developers of the method. The method is based on physisorption of an inert gas on the surface of the catalyst, until a monolayer has been formed. Nitrogen is the most common sorbate and the molecule occupies a surface area of 0.162 nm^2 at 77 K which is the boiling point of the gas. By measuring and calculating the amount of nitrogen it takes to form a monolayer at 77 K , the total surface area of the catalyst can be found. Equation 3 is developed from the Langmuir equation, and it is used to find the coverage of the adsorbed gas which is 1 in the case of a perfect monolayer.

$$\frac{P}{V(P_0 - P)} = \frac{P}{P_0} \frac{(\chi - 1)}{V_m \chi} + \frac{1}{V_m \chi} \quad (3)$$

In this equation V is the total volume of adsorbed gas at STP (Standard Temperature and Pressure) at pressure P . V_m is the volume of a monolayer of the adsorbed gas at STP, χ is the ratio between the heat of adsorption for the first layer and the next one and P_0 is the saturation pressure of the gas.

By plotting the left side of this equation against P/P_0 the result will be a straight line where V_m can be determined by the crossing of the y-axis. From this value, it is possible to calculate the total area of the adsorbed gas which equals the total area of the catalyst. During the experiment, the temperature is held constant at 77 K by nitrogen cooling while the partial pressure of N_2 is varied. The BET equation is built on the following assumptions [57]:

- The rate of adsorption and desorption in every layer is equal
- The heat of adsorption in the first layer is independent of the heat of adsorption in the next layers
- The heat of adsorption in the 2nd layer and up are equal and the same as the heat of liquefaction of the gas
- Monolayer and immobile adsorption
- Homogeneous surface, meaning that heat of adsorption is the same throughout entire catalyst and is independent of the coverage
- Dynamic equilibrium between the gas phase and the adsorbed species

These assumptions do not always hold true, but the BET method is very useful and the accuracy is usually good enough.

3 Experimental

3.1 Preparation of the catalyst

The incipient wetness point of P25 TiO_2 was found by measuring the amount of water it takes to wet a known mass of P25. The copper precursor was $\text{Cu}(\text{NO}_3)_2 \cdot 3\text{H}_2\text{O}$ and it was dissolved in just enough water to wet the P25 before 20 % more water was added. P25 was added gradually to the solution and the excess water made the mixture easier to work with and ensured an even distribution of the dissolved copper precursor. When all the P25 was added, the mixture had turned into a sticky and viscous porridge that was dried overnight at $70\text{ }^\circ\text{C}$ followed by crushing with mortar and pestle before undergoing calcination at $200\text{ }^\circ\text{C}$ for 4 hours. Picture 19 below shows how the unfinished catalyst looked before and after calcination.



Figure 19: The picture shows how the dried catalyst looked before (left) and after (right) the calcination process.

The color change from light-blue to dark grey indicates that the $\text{Cu}(\text{NO}_3)_2 \cdot 3\text{H}_2\text{O}$ has decomposed and CuO has been formed. The catalyst was crushed once more after calcination, before it was sieved through a custom-made sieve. The sieve was made by covering the opening of a beaker by a semi-stretched lady stocking of the type "La Mote Motelongs" which can be bought in almost any grocery store. The catalyst was added to the beaker before it was covered with the stocking, and catalyst was shaken through the sieve into a larger beaker.

The sieve set-up is shown in picture 20 below.



Figure 20: This is the equipment used for crushing and sieving.

The part of the catalyst that was rejected by the sieve was crushed once more before another sieving was performed. This was repeated one more time, with a total sieve count of three. The catalyst was then bottled and labelled according to its copper content and date.

3.2 Activity measurements

The cylindrical reactor was filled with a known mass of catalyst, a stirring magnet, 250 ml of distilled water and 250 ml of methanol. The lid was sealed and tightened before the reactor was put into the photochamber and connected to the gas tubes. The most essential part of the experimental set-up is shown on picture 21 below.

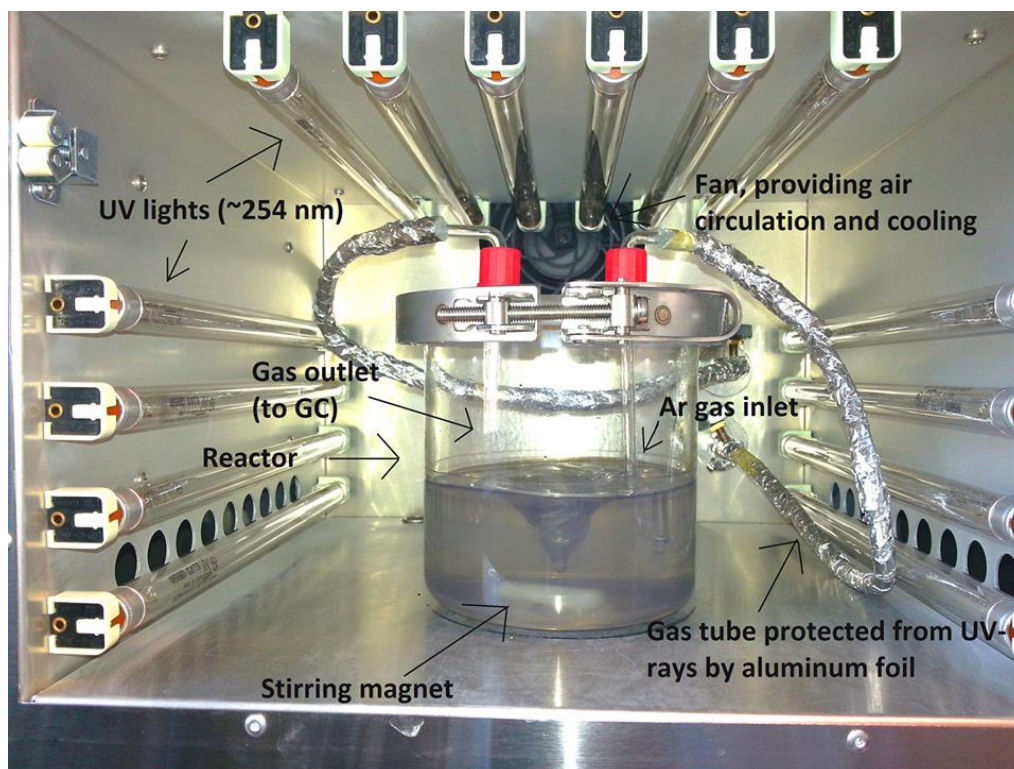


Figure 21: This is how experimental setup looks like.

The UV-lamps used are "Luzchem LZC-UVC" Hg-based where 88.6 % of the energy lies in the UVC region of 235-284 nm with a narrow peak at 254 nm. The rest are higher wavelengths ranging from 280-850 nm. The GC used is of the type "3000 micro GC" from Agilent Technologies. The chamber on the picture above has a door which was shut during every experiment.

Before the activity test was started by turning on the UV-light, the reaction mixture was flushed with an argon flow of 150 ml/min with stirring for 30 minutes. This was done in an attempt to remove dissolved oxygen from the liquid phase, which has the potential to disturb the photoreforming reaction. It took about 45 min before the first signs of hydrogen was detected by the GC and about 2 hours before a stable and realistic hydrogen concentration was detected. Much of this delay is caused by time it takes the gas to reach the GC, but it could also come from the fact that it may take the catalyst some time to reach its maximum activity. The experiment was repeated with different catalyst loadings between 10 mg and 1 g and with catalysts containing different mass percentage of copper ranging from 0 % to 10 %.

3.3 The challenge of obtaining reproducible results

The early goals of this project was to obtain information relating hydrogen evolution rate to catalyst loading and copper content. In an attempt to relate hydrogen evolution to catalyst loading, several activity tests were performed with different catalyst loadings. The problem with this approach was the fact that results made little sense and had no reproducibility. Before any results could be accepted, a way to obtain reproducible results from the experiments had to be found.

It was suspected that the poor reproducibility was mostly caused by the random distribution in grain size of the catalyst. After copper was impregnated on the P25 TiO₂ support and calcination was performed, some of the catalyst particles aggregated together to form larger clusters. If the tubes containing the photocatalyst was shaken, the larger clusters would gather at the top while the smaller particles would sink to the bottom. This is the same phenomena as in breakfast cereal where the largest grains are found on the top while the bottom of the cereal box often contains small sand-like particles which are usually not preferable. In the case of photocatalysis however, the smallest particles will have the largest specific surface area which gives them a good reason to be the preferable ones. Every time an experiment was conducted, the reactor contained some big grains which resembles sand and they sank rapidly to the bottom. Because the grains were big and gathered at the bottom of the reactor, they did not contribute much to the hydrogen evolution. Every activity experiment contained a different number of these low-activity sand-like grains, depending on how much the catalyst tube were shaken and exactly where in tube the catalyst were taken from.

This agglomeration problem had to be solved somehow and is showed picture 22 below.



Figure 22: This is how the agglomerated particles looked like at the bottom of the photoreactor.

The first proposed solution was sonication, where the biggest grains were gathered and sonicated to break the grains into smaller particles. This attempt was successful and sonification was performed on the entire reaction mixture before the activity was tested. While this solved the problem with the big grains, another problem arose. After a few hours of UV-light exposure, the reactor wall was completely covered in something that looked like dark catalyst mud, and metallic copper. This stopped light from penetrating through the reactor wall which heavily affected the incoming photon flux, preventing about 2/3 of total UV radiation from reaching the reaction mixture. To combat this problem, the layer was removed and the stirring speed was reduced in order to prevent the formation of a new layer on the wall. This worked well as a temporary fix because no new layer was formed, but it is likely that sonification somehow causes some copper to be removed from the support which is disadvantageous. Because sonification treatment produces local hotspots at nearly 5000 °C [58], it was suspected that reduction of copper started along with the sonication. Sonication without methanol was later attempted to prevent reduction of copper, but it gave the same result as before.

On picture 23 below, one can see how the reactor wall looked like after two hours on stream.

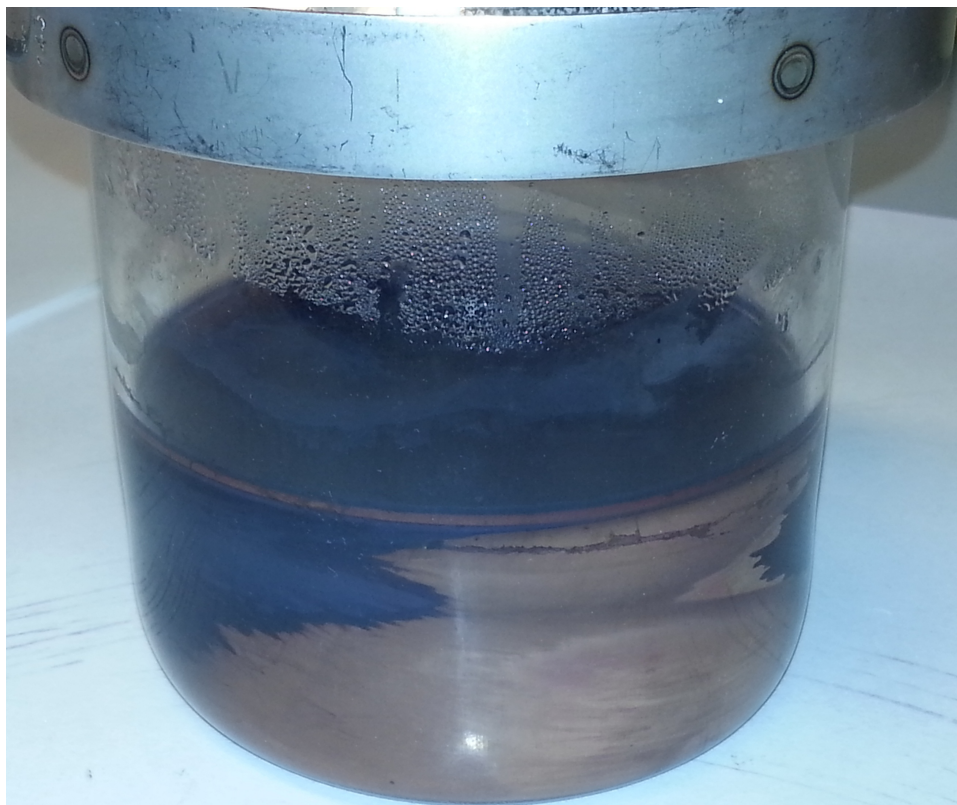


Figure 23: The picture shows how sonification pre-treatment causes metallic copper to settle on the reactor walls during the photoreforming reaction.

The sonification treatment is obviously too harsh for this photocatalyst, causing copper oxide to break loose from the titania support and in this way destroy the photocatalyst. It gets even worse when the the reducing enviroment during photoreforming causes copper oxide to undergo a reduction to metallic copper and settle on the walls, blocking a big portion of the incoming UV-light. It is likely that other preparation methods produces more solid photocatalysts where the semiconductor and the metal are harder to separate, but it is clear that the photocatalyst produced by the incipient wetness impregnation method is too weak to handle sonification. Because of this, another way of controlling the particle size had to be found.

The next proposed solution to the particle size problem was repeated crushing and sieving. The photocatalyst was crushed after calcination and sieved. The particles that were too big for the sieve was crushed again which prevented the biggest particles from being used in the experiments. The ideal way would perhaps be to use two sieves of different mesh size, and sort out both the largest and the smallest particles. This way, a middle fraction with a known minimum and maximum particle size could be used in every experiment and probably ensure good reproducibility. Unfortunately the advanced sieving equipment was already in use so a home-made solution had to be used. The applied sieving method and setup is described in detail in section 3.1, and the reproducibility of

the experiments increased dramatically with estimated relative errors ranging from 3.4 % to 7.3 % depending on catalyst loading.

3.4 Reactivation attempts

Because of decaying hydrogen evolution over time, several attempts were made in order to try and regain the catalyst activity. The first method that was attempted was hydrogen reduction. A catalyst loading of 1 g was selected and the photoreforming reaction was performed for around 20 hours. The UV-lamps were then turned off and hydrogen gas was bubbled through the reaction mixture at a rate of 5 ml/min together with 45 ml/min of argon gas for 30 min. The experiment was then re-started and the changes in hydrogen production rate was noted. The second method of reactivation was to refresh the reaction mixture by replacing the liquid phase and collect the catalyst in a filter so it could be used again. Vacuum filtering was used with a filter paper having a retention range of 4-12 μ g and the solution was repeatedly filtered through until it became blank. The reactor was cleaned, and 250 ml each of distilled water and methanol was added again. The catalyst caught in the filter was scraped off and the filter was washed thoroughly in the solution to make sure that as much photocatalyst as possible was recovered. The UV light was then switched on again and the experiment continued. This was repeated one more time before 250 ml extra methanol was added in the end. The results are showed in the next chapter.

3.5 BET measurements

BET analysis was performed in order to investigate the surface area of the different catalysts. The samples were degassed overnight in a Micromeritics VacPrep 061 at 110 °C and the mass before and after degassing was noted. During the first experiment, 200 °C was used as degassing temperature but this was too hot for the uncalcined sample which in fact got calcined during the degassing. The BET experiment itself was carried using N₂ adsorption on a Micromeritics Tristar 3000 Surface Area and Porosity analyzer.

4 Results and discussion

4.1 Activity measurements

4.1.1 The effect of catalyst loading on hydrogen generation

The catalyst loading was changed from 10 mg up to 1 g and the peak hydrogen generation rate was noted. The results are shown in figure 24 below.

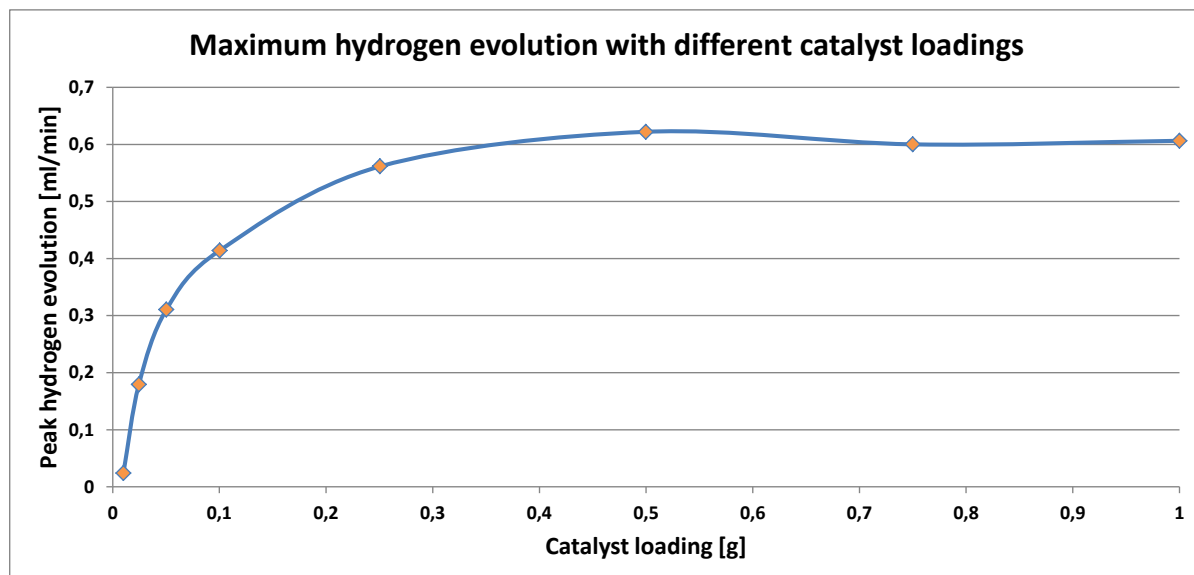


Figure 24: The graph shows how hydrogen generation rate depends on catalyst loading.

To the authors surprise, this graph does not seem to have any linear regions as opposed to what Herrmann [18] claims. This means that doubling the amount of catalyst would never double the hydrogen generation. The system seems to be saturated when the catalyst loading has reached about 0.5 g, meaning that adding extra catalyst beyond this point will not improve the hydrogen generation rate any further. If adding more catalyst after saturation does not improve the hydrogen generation rate, it probably means that all the UV-light is being adsorbed by the photocatalyst and there is nothing left for the extra catalyst added. It would be interesting to see if this catalyst saturation would happen at lower catalyst loadings if some of the 14 UV lamps were removed, but this would have to be done in the future because of time limitations.

The highest measured hydrogen generation rate was obtained when using 500 mg of the 10 wt.% Cu-TiO₂ photocatalyst, which produced 0.622 ml/min. This measurement was used to calculate that the quantum yield of the photocatalyst was at 0.41 %. This is not very impressive compared to other Cu-TiO₂ based photocatalysts, as an example Yu *et al.* has reported a quantum yield of 13.4 % [40]. The calculation is shown in Appendix A on page I.

Before a further discussion of this graph will take place, the calculated specific activity per gram catalyst will be presented. This was calculated from the different loadings by dividing the peak hydrogen production by the mass of catalyst in the reactor. The result is shown in the column chart at figure 25 below.

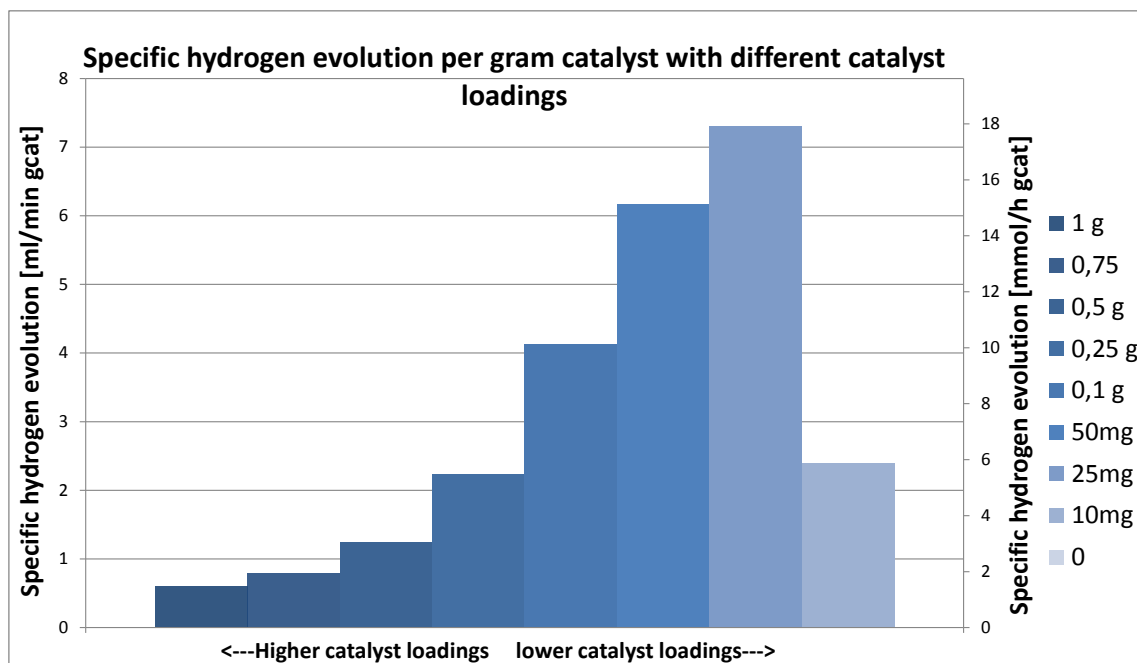


Figure 25: The graph shows how efficient each mass unit of the photocatalyst is at producing hydrogen under different catalyst loadings.

The column chart shows that each mass unit of catalyst is more effective at producing hydrogen when there are lower amounts of catalyst in the reactor. When the catalyst loading is low, the incoming photons created by the UV lamps will be shared by fewer catalyst particles compared to higher loadings. This gives each catalyst particle more available photons and as the figure shows, this increases the hydrogen generation rate per photocatalyst particle. At low catalyst loadings, the reaction rate of the photoreforming reaction seems to be something in between diffusion controlled and light-intensity controlled. This corresponds to the second regime, as described on page 13.

For the process to be truly diffusion controlled, the specific hydrogen generation per gram catalyst would flatten out as the catalyst loading was lowered. This point was not reached, and it is difficult and perhaps even impossible to reach it with the current experimental set-up. The reason is that there was not enough space for more UV-lamps. In theory one could think that by only adding a couple of catalyst particles to the reactor, the particles would be illuminated by high enough light-intensity to make the reaction diffusion controlled. This would probably fail in reality, because most of the photons would be adsorbed by the liquid phase, the reactor walls and the surroundings in general. The amount of produced hydrogen could also fall below the detection limit of the gas chromatograph.

When the catalyst loading increases, fewer and fewer photons are available per photocatalyst particle. This means the rate of electron and hole generation per particle would gradually decrease and ultimately fall below the rates of diffusion, adsorption and surface reaction 24. This means that for high catalyst loadings the system will be in the third regime where the reaction rate is light-intensity controlled and therefore proportional to the radiant flux of photons. As a result, the height of the plateau on the right in figure 24 should be proportional to the number of installed UV-lamps but there was not enough time to test this hypothesis.

On the column chart in figure 25, the very lowest catalyst loading of 10 mg breaks the general trend and this is not easy to explain. The measurement was repeated three times with a relative error of 7.3 %, meaning that it was not just some a random failure that caused the strange measurement. One possible explanation could be that the gas chromatograph struggles at finding or calculating the correct amount of hydrogen when the gas is highly diluted which happens at very low catalyst loadings. Other unknown effects could also be the cause.

4.1.2 The effect of copper content on the photocatalytic activity of Cu–TiO₂

In several studies, the optimum copper content of the Cu–TiO₂ photocatalyst is reported to be everywhere from 1.2 wt.% to 8.12 wt.%. Seven different catalyst were synthesized using the wetness impregnation method, having a copper content ranging from 0 wt.% to 10 wt.%. Two different 0 wt% Cu catalyst were tested, one of them was pure and untreated P25 while the other one received the same treatment as the copper catalysts except the addition of the copper precursor to the impregnation water. None of these two catalysts produced any detectable amount of H₂ during the photoreforming reaction, meaning that a co-catalyst such as copper is crucial for the photoactivity of the TiO₂ catalyst. In order to determine the optimum copper content the catalyst was loaded with 250 mg of catalyst and the detailed procedure is already explained in section 3.2 on page 35. In figure 26 below, the peak hydrogen evolution of the different catalyst is plotted against wt.% Cu.

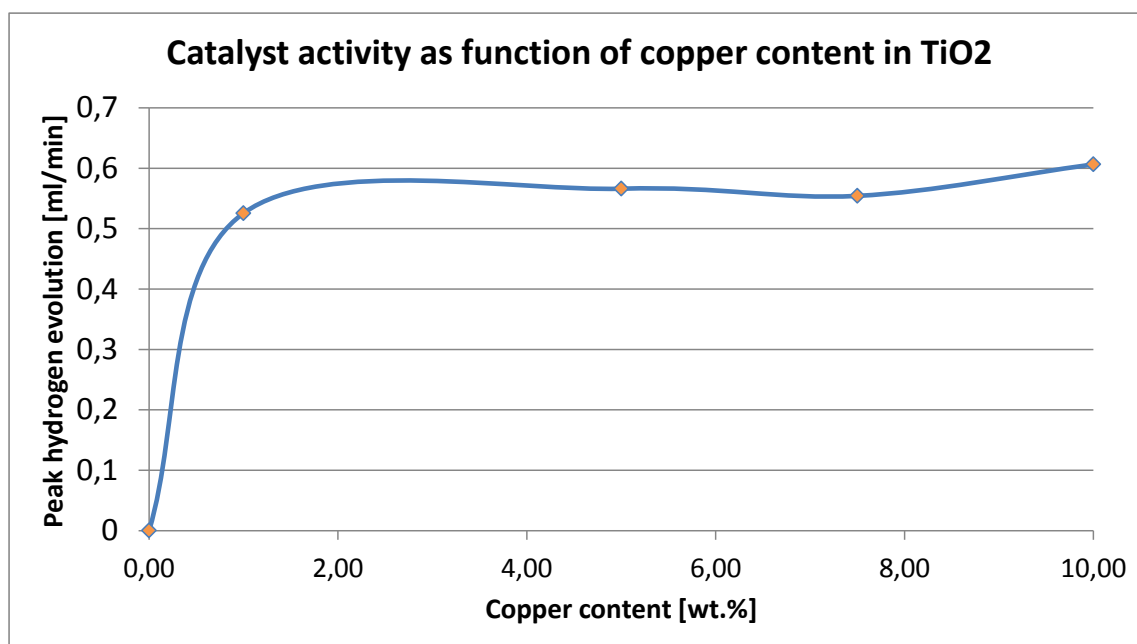


Figure 26: The graph shows how the copper content of the Cu–TiO₂ photocatalyst affects the photocatalytic activity.

The figure shows that as long as there are some copper species present, the exact amount seems to be of little importance to the activity of the photocatalyst. The best result was achieved with 10 wt.% Cu, but with such small margins nothing can really be concluded yet.

The shape of the figure above differs significantly from what is obtained by Wu *et al.* and from figure 14 on page 23 obtained by Sreethawong and Yoshikawa [37], where the activity of the Cu–TiO₂ photocatalyst drops significantly after only 1.2 wt.% and 1.5 wt.% Cu respectively. It is likely that the difference in results are caused by a different preparation method of the catalyst. The catalyst used in this project was prepared using

the incipient wetness impregnation method (IWI), while Sreethawong and Yoshikawa used a single-step sol-gel method. From table 1 on page 22 it seems like there is a slight trend where the reported optimal Cu loading generally is lower for sol-gel method than for IWI method. In 2011 Ida Bjørnstad reported in her Master's Thesis that the CuO tend to be deposited in the pores of the titania particles when the IWI method was used, while a higher percentage of the CuO was deposited on the particle surface when other methods like the deposition precipitation (DP) method was used [50]. This coincides very well with the fact that Cu–TiO₂ photocatalysts seems to have higher "copper tolerance" when they are prepared using the IWI method. When a high percentage of the copper oxide is deposited inside the pores of the titania particles, they are deposited in the "shadow zone" where they do not block incoming photons from hitting the titania phase while they are still able participate in the reaction. On the other hand, CuO deposited on the surface of the titania will block some of the incoming photons from reaching the titania phase and in this way limit the photoactivity of the catalyst. In short, the IWI method can handle higher copper contents because most of the copper doesn't block photons from reaching the TiO₂ phase. Because of time limitations however, no catalysts were made by the DP method meaning that this theory was not verified.

4.2 Catalyst deactivation and reactivation attempts

One of the activity experiments were run for an extended amount of time, in order to see much the catalyst would deactivate. The graph on figure 27 below shows how the activity of the photocatalyst decays with time after the peak activity is reached.

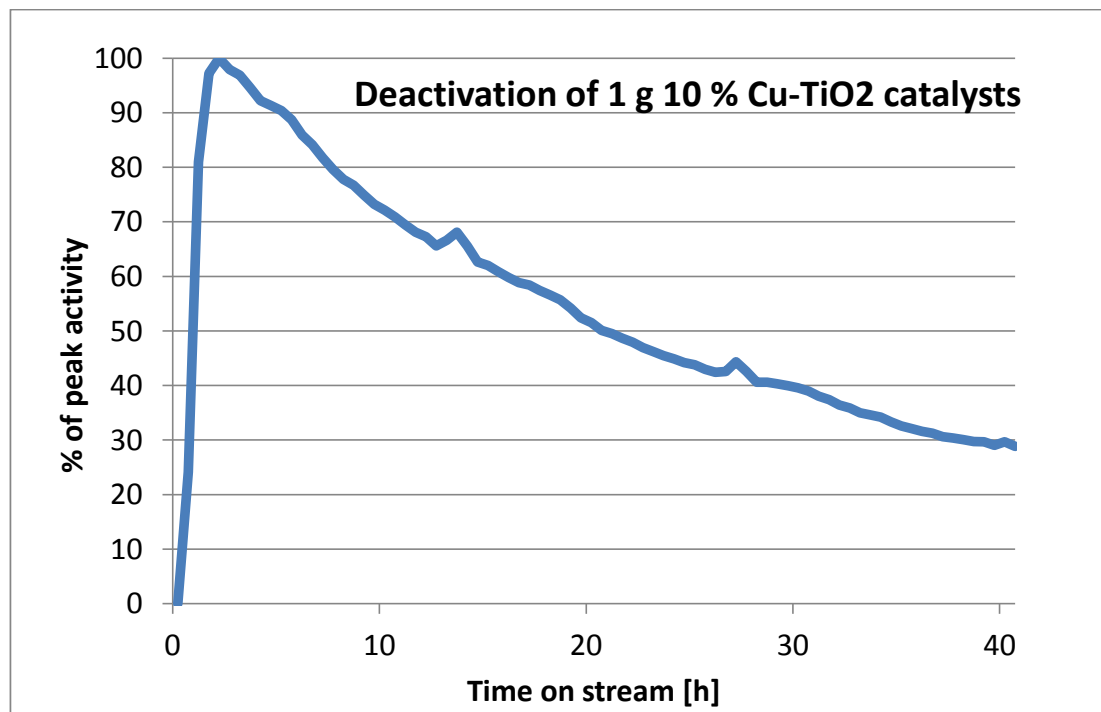


Figure 27: The figure shows how the hydrogen production decays over time as the photocatalyst deactivates.

As the graph shows, the photocatalytic system suffered from deactivation and the hydrogen generation rate dropped from 100 % to 50 % in about 19 hours. After about 40 hours, only 30 % of the peak activity was left.

As mentioned on page 39, hydrogen reduction was attempted in order to recover some of the photocatalytic activity. This had no effect at all, indicating that oxidation of the catalyst is not a problem. This should not really come as any surprise, as the methanol ensures that the liquid phase provides a reducing environment.

The other method that was attempted was much more successful. The liquid phase was renewed two times and an extra 250 ml of methanol was added the third time in order to observe how the photocatalytic activity responded. The photocatalyst was never cleaned during the experiment and the results are shown in figure 28 below.

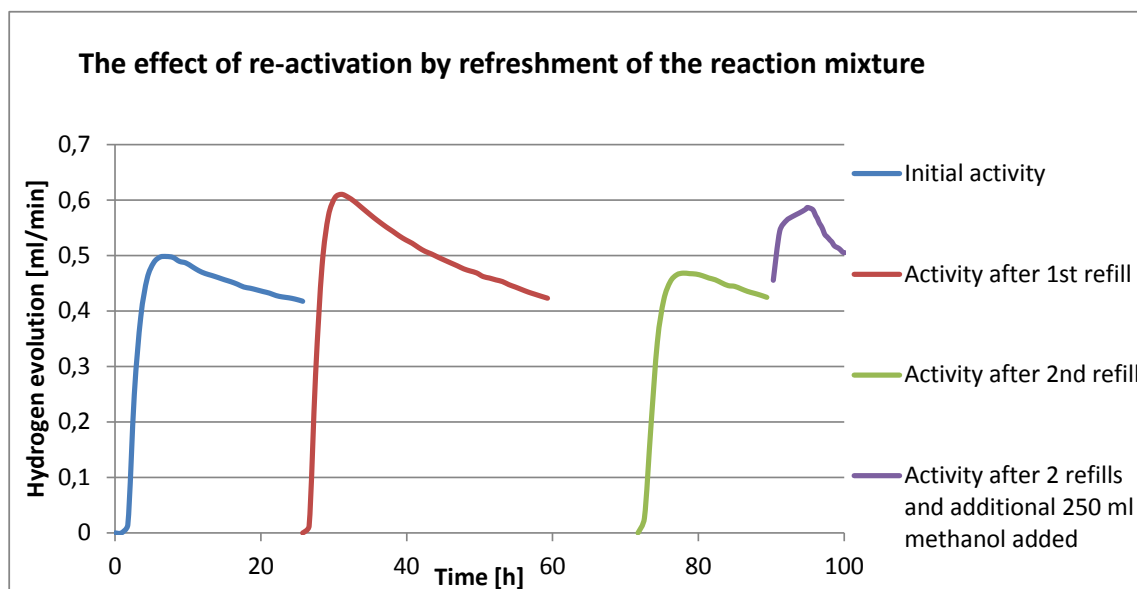


Figure 28: The figure shows how the hydrogen evolution responds to refreshment of solution and the addition of more methanol.

The figure shows varying results from refreshing the liquid phase. The first time it increases the activity beyond the previous maxima while the second time shows a much weaker effect. The fact that the activity is increased beyond the first maxima is not easy to explain, but it might suggest that there are both deactivation mechanisms and activation mechanisms occurring at the same time. It could be that accumulation of by-products has a deactivating effect while there are some other effects that activate the catalyst. Every time after a photoreforming experiment was performed, the catalyst and reactor smelled a bit like fish, which is probably caused by one or several by-products. The fact that refreshment of the solution worked so well even though the catalyst was not cleansed, suggests that the major source of deactivation actually is the accumulation of by-products which are not strongly adsorbed on the photocatalyst. This coincides well with what Xu *et al.* has reported in literature where accumulation of by-products was found to be the largest source of deactivation [3]. On picture 23 on page 38, the reduction of copper oxides to metallic copper is confirmed and this is also a contributor to deactivation even though it is hard to say exactly to which extent this occurs.

One of the activating effects could be caused when excited electrons accumulate in the TiO_2 phase causing the particles to receive a local negative charge in the bulk phase. In order to preserve the overall electroneutrality of the particles, H^+ ions are likely to stick to the particle surface giving the particle a positive surface charge. This positive surface charge could cause repulsive forces between the particles and in this way separate those

who have agglomerated. Agglomeration has been present in every experiment and is observable with the naked eye as shown on figure 22 on page 37. If these agglomerations were to break into smaller particles, the overall active surface area should increase which would boost the hydrogen evolution. Another activating effect could be the removal of dissolved oxygen from the liquid phase caused by the continuous argon flow and perhaps also depletion by reaction. Dissolved oxygen may react with the excited electrons in place of H^+ and thus inhibit hydrogen generation.

The dominant source of error for this particular experiment is likely to be the fact that some catalyst is lost in the filtering process. This amount is probably not the same every time, and it is the smallest and most active particles that are the hardest one to recover because they stick very well to the filter. This reduced the catalyst loading every time filtration was performed. It is possible that more catalyst was lost during the 2nd filtering process than during the first, but it is hard to tell. It could also be that the activating effect was completed and stopped before the 2nd refreshment of the solution. When it comes to the addition of extra methanol, Xu *et al.* argues that the hydrogen evolution increases with methanol concentration according to the Freundlich adsorption isotherm so the obtained result is not surprising [41].

On a second note, the photoreforming was run at a very high catalyst loading which means that a slight decrease in the loading should have negligible effect on the hydrogen evolution rate. This is illustrated well on figure 24 on page 40 where the catalyst loadings correspond to the plateau-area of the graph even after some catalyst is lost. This makes it hard to say if losing some of the smallest catalyst particles really has any effect on the hydrogen production rate.

4.3 Additional observations

On figure 25, the last measurement breaks the overall trend. By assuming that this was caused by an error and changing the value to something more expected, figure 29 below was created.

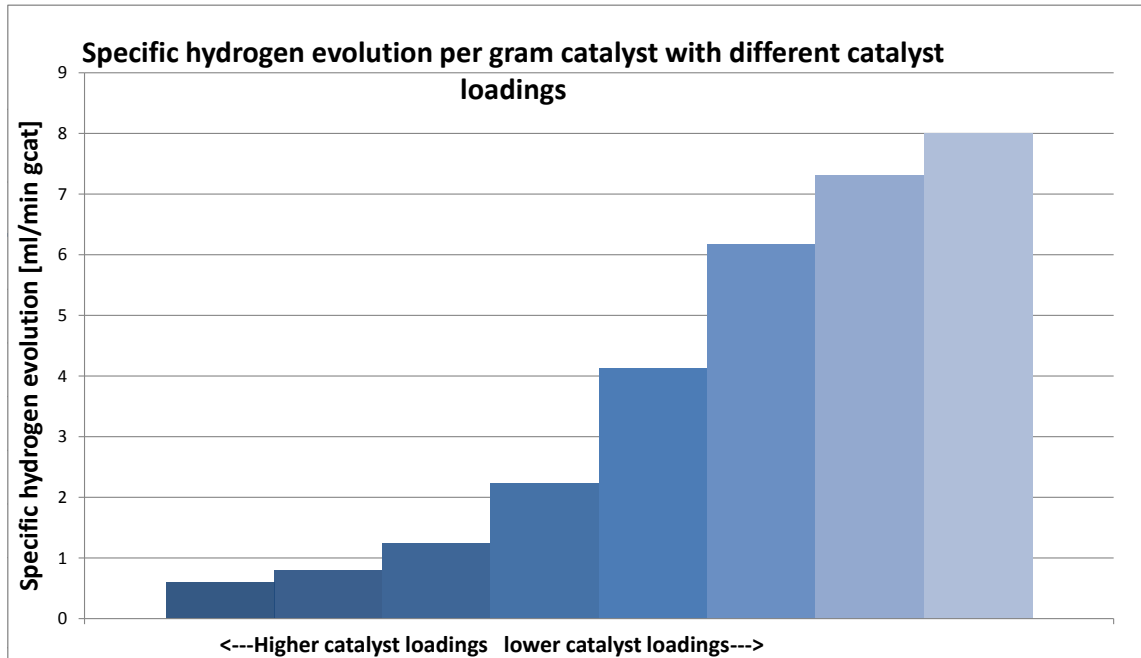


Figure 29: The graph shows how efficient each mass unit of the photocatalyst is at producing hydrogen under different catalyst loadings.

The column to the right in the chart above changed from the original value of 2,4 to 8 which is a fabricated value, but the chart looks nicer and more systematic this way.

If the same value is used to replace the old value on figure 24, the graph would like look like figure 30 below.

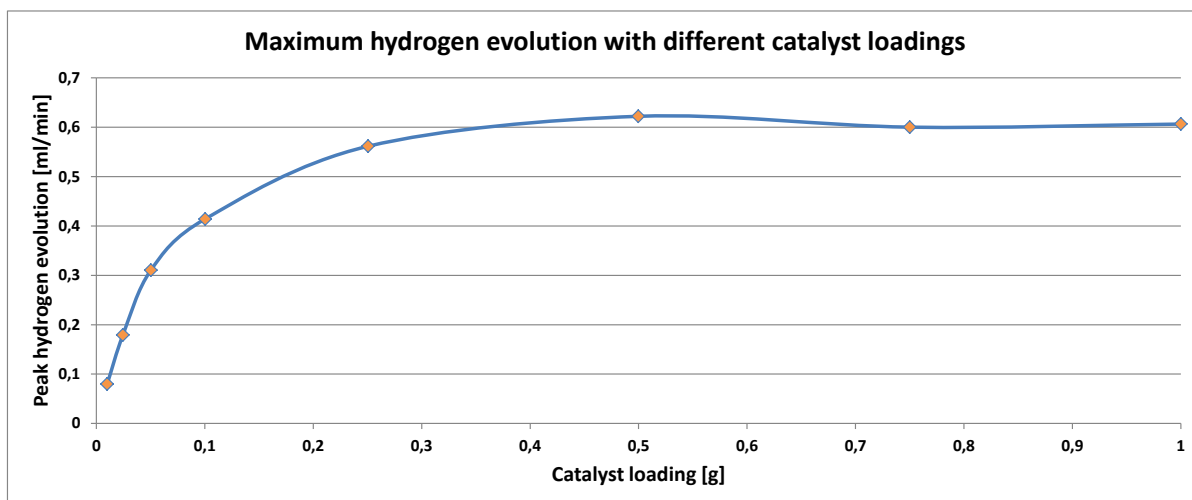


Figure 30: The graph shows how hydrogen generation rate depends on catalyst loading.

An interesting observation is that the three first points on the graph appear to be on a straight linear line. To better see if this really is the case, figure 31 has zoomed in on the four first points of the the graph:

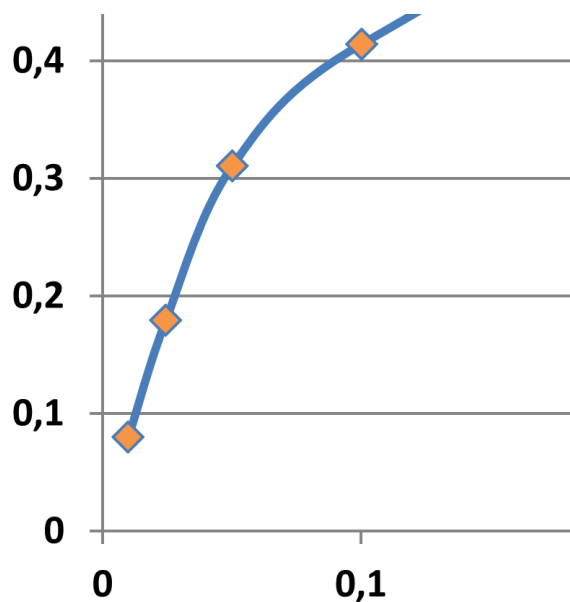


Figure 31: Magnification of four first points of graph 30.

Indeed the three first points seem to be approximately on a linear line, which agrees well with what Herrmann has reported [18].

A final observation was done by setting an arbitrary value for the total light flux, and then divide the catalyst loading with this number. Specific hydrogen generation was plotted against this value, creating a graph that shows how much hydrogen each mass unit of the catalyst produces at different light intensities. The graph is shown in figure 32 below.

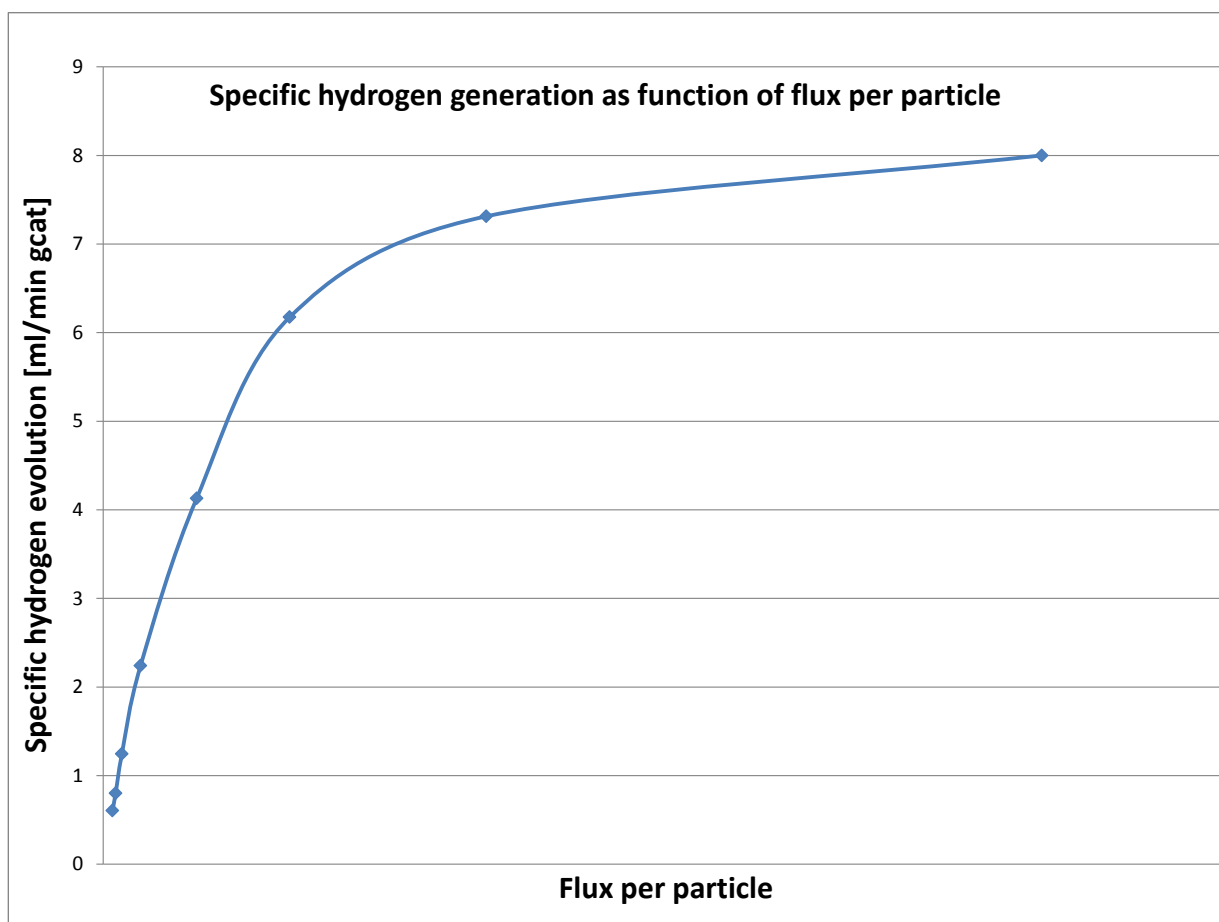


Figure 32: The graph shows how hydrogen generation per mas unit of catalyst is related to the incoming photon flux.

The graph shows that at high catalyst loadings (left side of the graph), the reaction rate scales almost linearly with the radiant flux. At lower catalyst loadings (right side of the graph), the light intensity is no longer the bottleneck and the the rate of diffusion and adsorption of methanol becomes important. It is important to realize that the values on the x-axis are only estimated and the accuracy of these values decreases with increasing values of x. The reason for this is the fact that the percentage of photons who are adsorbed by the environment instead of the catalyst particles, increased with decreased catalyst loadings. This graph is another indication that the third reaction rate regime (fully diffusion controlled) is never quite reached in these experiments, as the slope does not fully flattens out.

4.4 Choosing the appropriate values to report

As seen on figure 25, the specific hydrogen production rate of the 10 wt.% Cu–TiO₂ photocatalyst is ranging from 1.49 to 17.93 mmol h⁻¹ g_{cat.}⁻¹ depending on the catalyst loading. It could of course be tempting to report the highest value, if the goal was to obtain research funding and getting a reputation. As it stands today, reporting the highest value actually seems to be accepted even though the corresponding catalyst loading is as low as 25 mg per 0.5 L which is very unrealistic for a commercialized process. According to Herrmann [18] the field of heterogeneous photocatalysis has only reached the pre-industrial level. Most of the scientific articles in the field are written by physicians and chemists, not by chemical engineers or entrepreneurs who craves commercialisation. As a result, there are no standardised guidelines for how the experiments should be conducted and how to report the results. In the abstract-, results- and conclusions part of the scientific articles where a specific hydrogen generation rate is reported, this value is always reported alone without information about the corresponding catalyst loading. The information regarding catalyst loading is usually only found by searching through the experimental part of such an article. In other words, the two closely related numbers of catalyst loading and specific hydrogen generation are not reported together. One could actually argue that this makes the reported value of specific hydrogen generation rate less informative and trustworthy than what it seems like at first glance.

The author would like to propose a simplified solution to this problem, that neither requires too much time nor the acquisition of new lab-equipment. The perfect solution to making standardised measurements and reports, would of course be to use standardised equipment and a standardised catalyst loading. This is very unrealistic, as different labs operates with different reactors and radiant fluxes. A simplified solution to the problem could– be to just report the initial quantum yield with respect to hydrogen , the quantum yield after 24 hours or a set number of hours/days and the corresponding wavelength of the light source. This is probably the best way to compare photocatalysts, as the results should in theory be independent of the equipment used. Luckily the quantum yield and the corresponding wavelength are to some extent used in literature today, usually as a means to determine the quality of novel photocatalysts like for example K₄Nb₆O₁₇ as reported by Domen *et al.*

If one still insists on reporting a hydrogen generation rate, this could be done in a fair way by first finding the catalyst saturation point of the system. This is done by conducting experiments on different catalyst loadings and producing a graph like figure 24 on page 40. The reported specific hydrogen generation rate should be the value obtained at catalyst saturation of the system. This is reasonable because a future commercialized photoreforming process would have to be operated as cost-efficient as possible, which is obtained when the catalyst loading is at the saturation point. At this optimum catalyst loading, the hydrogen production per plant is maximized with a minimal waste of catalyst. The catalyst saturation point is also likely to adjust itself from one radiant flux to another, making sure that experimental set-ups do not gain any advantage or disadvantage by using a different number of UV-lamps. A final detail that should also be reported along with the hydrogen evolution rate, is the wavelength of the light source

that has been used, or atleast information about how large percentage of the photons which are able to overcome the bandgap of the semiconductor. A high hydrogen production at higher wavelength is more impressive than at low wavelengths. By using this standardised method, the reader would get a better impression of the real quality of the photocatalyst.

In this project, the catalyst saturation point was at 500 mg and the corresponding specific hydrogen generation rate was measured to be $3.05 \text{ mmol h}^{-1} \text{ g}_{\text{cat.}}^{-1}$. If this was a scientific article, the reported value would then be "3.05 $\text{mmol h}^{-1} \text{ g}_{\text{cat.}}^{-1}$ at catalyst saturation (500 mg cat.) with a quantum yield of 0.41 % using UVC light at 254 nm". By implementing this convention, sorting out the better photocatalyst from the worse could be done faster, easier and maybe even the commercialisation of photoreforming would speed up.

4.5 BET results

The results from the BET measurements are shown in table 2 below.

Table 2: The table shows the measured BET surface area for the different Cu–TiO₂ catalysts.

Sample	P25	0 wt.% Cu	1 wt.% Cu	5 wt.% Cu	10 wt.% Cu
BET surface area [m ² g ⁻¹]	53.6	53.3	53.5	49.8	44.7

The results show that the BET surface area is decreasing slightly when the amount of copper is increased. This observation agrees with Sreethawong and Yoshikawa's [37] observations and was therefore expected. The difference between the P25 sample and the "0 wt.% Cu" is that the latter sample has received the same treatment as the other Cu–TiO₂ catalysts with the exception of adding the copper precursor to the distilled water. Because the results are so similar, it looks like wetting, drying and calcination at 200 °C for 4 h does not affect the surface area of the TiO₂ phase. This may come as a surprise because the two samples look quite different, the pure P25 sample is very light and "fluffy" whereas the calcined sample is much more dense.

5 Conclusions

Cu–TiO₂ catalysts prepared by the IWI method consists of particles that tend to agglomerate strongly, so proper crushing and sieving of the photocatalyst powder is necessary for getting reproducible results during photoreforming experiments.

The specific hydrogen generation rate was observed to increase with decreasing catalyst loading, due to higher photon flux per mass unit of photocatalyst. The reaction kinetics seemed to be mainly controlled by the light intensity, but for low catalyst loadings it seems like the kinetics started to approach the diffusion controlled domain.

The pure TiO₂ photocatalyst did not produce any detectable amount of H₂, but the hydrogen generation rates of the catalysts containing 1 wt.% Cu, 5 wt.% Cu, 7.5 wt.% Cu and 10 wt.% Cu were surprisingly similar. The weak copper dependency illustrated by figure 26 does not agree well with literature [38] [37], but this difference is likely to be caused by the difference in catalyst preparation methods.

The system used in this project was saturated with photocatalyst at a catalyst loading of 500 mg. At this point, the specific hydrogen generation was measured to be 3.05 mmol h⁻¹ g_{cat.}⁻¹ and the quantum yield was calculated to be at 0.41 %.

The photocatalytic system suffered from deactivation and the hydrogen generation rate dropped from 100 % to 50 % in about 19 hours. Among the reactivation attempts, refreshment of the liquid phase was highly successful in regaining the lost activity. This indicates that the main source of deactivation comes from the accumulation of by-products, even though the reduction of Cu_xO to metallic Cu is confirmed on picture 23.

The BET surface area of the catalyst was unaffected by the IWI method and the calcination itself, but an increasing copper content caused a decreasing BET surface area.

6 Future work

If a continuation of this project or a similar project will be carried out in the future, several improvements could and should be made. The first improvement that comes to mind is the replacement of the custom-made sieve having a large but variable mesh-size by two proper ones with a known and constant mesh-size. This way, one could use a middle fraction of the photocatalyst where the particles have a known minimum and maximum size. This should increase the reproducibility of the photoreforming experiments even further by eliminating the randomness in particle size.

The plateau at figure 24 on page 40 started at a catalyst loading of 500 mg, and it would be really interesting to see if this plateau would be moved to a lower catalyst loading by removing some of the UV-lights. The optimal copper loading could also be found for catalysts made by other methods than the IWI method, to confirm if this value really depends on the preparation method or not.

There is also more to be done about the investigations on deactivation. The extent of CuO reduction could be investigated along with an analysis of the by-products. Maybe the stability of the process could be improved by adding a reagent that reacts with the byproducts?

References

- [1] J. Blanco et al. Renewable and sustainable energy reviews 13. 13:1437, 2009.
- [2] BP. Consumption by fuel, 1965–2008. *Statistical Review of World Energy*, 2008.
- [3] Shiping Xu, Jiawei Ng, Xiwang Zhang, Hongwei Bai, and Darren Delai Sun. Fabrication and comparison of highly efficient cu incorporated TiO₂ photocatalyst for hydrogen generation from water. *International Journal of Hydrogen Energy*, 35(11):5254 – 5261, 2010. 3rd Argentinean and 2nd Latin American Congress in Hydrogen and Sustainable Energy Sources.
- [4] A. Domínguez, J.A. Menéndez, and J.J. Pis. Hydrogen rich fuel gas production from the pyrolysis of wet sewage sludge at high temperature. *Journal of Analytical and Applied Pyrolysis*, 77(2):127 – 132, 2006.
- [5] Susanta K. Das, Antonio Reis, and K.J. Berry. Experimental evaluation of co poisoning on the performance of a high temperature proton exchange membrane fuel cell. *Journal of Analytical and Applied Pyrolysis*, 2009.
- [6] Ilenia Rossetti. Hydrogen production by photoreforming of renewable substrates. *ISRN Chemical Engineering*, 2012.
- [7] Paul Alois. Global water crisis overview. <http://www.arlingtoninstitute.org/wbp/global-water-crisis/441>. Accessed: 10/04/2013.
- [8] U.S. DEPARTMENT OF ENERGY. Toward a Hydrogen Economy. http://www.netl.doe.gov/keyissues/hydrogen_economy.html. Accessed: 9/06/2013.
- [9] McNaught and Wilkinson. Iupac gold book - photocatalyst. <http://goldbook.iupac.org/PT07446.html>. Accessed: 30/02/2013.
- [10] B. Ohtani. Photocatalysis A to Z—what we know and what we do not know in a scientific sense. *Journal of Photochemistry and Photobiology C: Photochemistry Reviews*, 11(4):157 – 178, 2010.
- [11] Akira Fujishima, Xintong Zhang, and Donald A. Tryk. TiO₂ photocatalysis and related surface phenomena. *Surface Science Reports*, 63(12):515 – 582, 2008.
- [12] KENICHI HONDA AKIRA FUJISHIMA. Electrochemical photolysis of water at a semiconductor electrode. *Nature*, (5358):37–38, 1972.
- [13] Hilde Venvik, editor. *TKP 4515 KEM 2012 Photocatalysis*. NTNU, SINTEF, 2012. With input from Magnus Rønning, Astrid Mejdell and Asmira Delic.
- [14] Kazuya Nakata and Akira Fujishima. TiO₂ photocatalysis: Design and applications . *Journal of Photochemistry and Photobiology C: Photochemistry Reviews*, 13(3):169 – 189, 2012.
- [15] Akira Fujishima, Xintong Zhang, and Donald A. Tryk. TiO₂ photocatalysis and related surface phenomena. *Surface Science Reports*, 63(12):515 – 582, 2008.

- [16] Chong-Mou Wang, Adam Heller, and Heinz Gerischer. Palladium catalysis of O₂ reduction by electrons accumulated on TiO₂ particles during photoassisted oxidation of organic compounds. *Journal of American Chemical Society*, 13(114):5230–5234, 1992.
- [17] H. S. Fogler. *Elements of Chemical Reaction Engineering*. Prentice Hall, New Jersey, 3 edition, 1999.
- [18] J.-M. Herrmann. Heterogeneous photocatalysis: state of the art and present applications in honor of pr. r.l. burwell jr. (1912–2003), former head of ipatieff laboratories, northwestern university, evanston (ill). *Topics in Catalysis*, 34(1-4):49–65, 2005.
- [19] Hasliza Bahruji, Michael Bowker, Philip R. Davies, and Fabien Pedrono. New insights into the mechanism of photocatalytic reforming on Pd–TiO₂. *Applied Catalysis B: Environmental*, 107(1–2):205 – 209, 2011.
- [20] Kazuhito Hashimoto, Hiroshi Irie, and Akira Fujishima. TiO₂ photocatalysis: A historical overview and future prospects. *Japanese Journal of Applied Physics*, 44(12):8269–8285, 2005.
- [21] Kazuhito Hashimoto, Hiroshi Irie, and Akira Fujishima. TiO₂ photocatalysis: A historical overview and future prospects. *Japanese Journal of Applied Physics*, 44(12):8269–8285, 2005.
- [22] N. T. Nolan, M. K. Seery, and S. C. Pillai. Spectroscopic investigation of the anatase-to-rutile transformation of sol-gel-synthesized TiO₂ photocatalysts. *Journal of Physical Chemistry C*, 113(36):16151–16157, 2009. Cited By (since 1996): 22.
- [23] Y. Hu, H. . Tsai, and C. . Huang. Effect of brookite phase on the anatase-rutile transition in titania nanoparticles. *Journal of the European Ceramic Society*, 23(5):691–696, 2003. Cited By (since 1996): 86.
- [24] *Complexes and First-Row Transition Elements*. MacMillan Education, 1974.
- [25] Miguel Pelaez, Nicholas T. Nolan, Suresh C. Pillai, Michael K. Seery, Polycarpus Falaras, Athanassios G. Kontos, Patrick S.M. Dunlop, Jeremy W.J. Hamilton, J.Anthony Byrne, Kevin O’Shea, Mohammad H. Entezari, and Dionysios D. Dionysiou. A review on the visible light active titanium dioxide photocatalysts for environmental applications. *Applied Catalysis B: Environmental*, 125(0):331 – 349, 2012.
- [26] A. Wisitsoraat, A. Tuantranont, E. Comini, G. Sberveglieri, and W. Wlodarski. Characterization of n-type and p-type semiconductor gas sensors based on niox doped TiO₂ thin films. *Thin Solid Films*, 517(8):2775 – 2780, 2009.
- [27] Michael R. Hoffmann, Scot T. Martin, Wonyong. Choi, and Detlef W. Bahnemann. Environmental applications of semiconductor photocatalysis. *Chemical Reviews*, 95(1):69–96, 1995.

- [28] Yawen Wang, Yu Huang, Wingkei Ho, Lizhi Zhang, Zhigang Zou, and Shuncheng Lee. Biomolecule-controlled hydrothermal synthesis of C–N–S-tridoped TiO₂ nanocrystalline photocatalysts for NO removal under simulated solar light irradiation. *Journal of Hazardous Materials*, 169(1–3):77 – 87, 2009.
- [29] C. Su, C.-M. Tseng, L.-F. Chen, B.-H. You, B.-C. Hsu, and S.-S. Chen. Sol–hydrothermal preparation and photocatalysis of titanium dioxide. *Thin Solid Films*, 498(1–2):259 – 265, 2006. Proceedings of The Third Asian Conference on Chemical Vapor Deposition (Third Asian-CVD).
- [30] Tom’s of Maine. Ingredients: Titanium dioxide. <http://www.tomsomaine.com/research/ingredients/ingredient-detail/titanium-dioxide>. Accessed: 24/04/2013.
- [31] Winkler and Jochen. *Titanium Dioxide*. Vincentz Network, 2003.
- [32] K Joseph Anthony Raj and B Viswanathan. Effect of surface area, pore volume and particle size of p25 titania on the phase transformation of anatase to rutile. *Indian Journal of Chemistry*, 2009.
- [33] Jae Sung Lee. Nanocomposite photocatalysts for solar hydrogen production.
- [34] Maria Vittoria Dozzi and Elena Selli. Doping TiO₂ with p-block elements: Effects on photocatalytic activity. *Journal of Photochemistry and Photobiology C: Photochemistry Reviews*, 14(0):13 – 28, 2013.
- [35] Ulrike Diebold. Photocatalysts: Closing the gap. *Nature Chemistry*, 3(4):271–2, 2011. Copyright - Copyright Nature Publishing Group Apr 2011; Last updated - 2013-02-23; DOI - 2344476471; 61266581; 145835; NCHM; 21430683.
- [36] X. Chen, L. Liu, P. Y. Yu, and S. Mao. Increasing solar absorption for photocatalysis with black hydrogenated titanium dioxide nanocrystals. *S. Science*, 331:746–750, 2011.
- [37] Thammanoon Sreethawong and Susumu Yoshikawa. Comparative investigation on photocatalytic hydrogen evolution over Cu-, Pd-, and Au-loaded mesoporous TiO₂ photocatalysts. *Catalysis Communications*, 6(10):661 – 668, 2005.
- [38] Nae-Lih Wu and Min-Shuei Lee. Enhanced TiO₂ photocatalysis by Cu in hydrogen production from aqueous methanol solution. *International Journal of Hydrogen Energy*, 29(15):1601 – 1605, 2004.
- [39] Hyung-Joo Choi and Misook Kang. Hydrogen production from methanol/water decomposition in a liquid photosystem using the anatase structure of Cu loaded TiO₂. *International Journal of Hydrogen Energy*, 32(16):3841 – 3848, 2007. Symposium on Materials in Clean Power Systems.
- [40] Jianguo Yu, Yang Hai, and Mietek Jaroniec. Photocatalytic hydrogen production over CuO-modified titania. *Journal of Colloid and Interface Science*, 357(1):223 – 228, 2011.

- [41] Shiping Xu and Darren Delai Sun. Significant improvement of photocatalytic hydrogen generation rate over TiO_2 with deposited CuO . *International Journal of Hydrogen Energy*, 34(15):6096 – 6104, 2009.
- [42] J. Bandara, C.P.K Udawatta, and C. S. K. Rajapakse. Highly stable CuO incorporated TiO_2 catalyst for photocatalytic hydrogen production from H_2O . *Photochemical and Photobiological Sciences*, 2005.
- [43] Shiping Xu and Darren Delai Sun. Significant improvement of photocatalytic hydrogen generation rate over TiO_2 with deposited CuO . *International Journal of Hydrogen Energy*, 34(15):6096 – 6104, 2009.
- [44] Maria D., Hernandez-Alonso, Fernando Fresno, Silvia Suarez, and Juan M. Coronado. Development of alternative photocatalysts to TiO_2 : Challenges and opportunities. *Energy & Environmental Science*, 2009.
- [45] Hideki Kato, Kiyotaka Asakura, and Akihiko Kudo. Highly efficient water splitting into H_2 and O_2 over lanthanum-doped NaTaO_3 photocatalysts with high crystallinity and surface nanostructure. *Journal of the American Chemical Society*, 125(10):3082–3089, 2003.
- [46] Akihiko Kudo, Hideki Kato, and Seira Nakagawa. Water splitting into H_2 and O_2 on new Sr_2MO_7 ($\text{M} = \text{Nb}$ and Ta) photocatalysts with layered perovskite structures: Factors affecting photocatalytic activity. *The Journal of Physical Chemistry B*, 104(3):571–575, 2000.
- [47] HyunGyu Kim, DongWon Hwang, SangWon Bae, JongHyeon Jung, and JaeSung Lee. Photocatalytic water splitting over $\text{La}_2\text{Ti}_2\text{O}_7$ synthesized by the polymerizable complex method. *Catalysis Letters*, 91(3-4):193–198, 2003.
- [48] S. Ikeda, M. Hara, J.N. Kondo, K. Domen, H. Takahashi, T. Okubo, and M. Kakihana. Preparation of $\text{K}_2\text{La}_2\text{Ti}_3\text{O}_{10}$ by polymerized complex method and photocatalytic decomposition of water. *Chemistry of Materials*, 10(1):72–77, 1998. cited By (since 1996)101.
- [49] Catherine Louis. Production of Supported Catalysts by Impregnation and (Viscous) Drying. <http://www.crcnetbase.com/doi/pdf/10.1201/9781420006506.ch15>. Accessed: 11/06/2013.
- [50] Ida Lien Bjørnstad. Photocatalytic fuel production by photoreforming of hydrocarbons. Master’s thesis, NTNU - Norwegian University of Technology and Science, 2011.
- [51] The Free Dictionary. calcination. <http://www.thefreedictionary.com/calcination>. Accessed: 3/06/2013.
- [52] Catherine Louis. Deposition-Precipitation Synthesis of Supported Metal Catalysts. <http://www.crcnetbase.com/doi/pdf/10.1201/9781420006506.ch14>. Accessed: 3/06/2013.

- [53] Catherine Louis. Sol-gel methods. http://www.uio.no/studier/emner/matnat/kjemi/KJM5100/h06/undervisningsmateriale/10KJM5100_2006_sol_gel_d.pdf. Accessed: 3/06/2013.
- [54] Joe Satcher. Novel Materials from Solgel Chemistry. <https://www.llnl.gov/str/May05/Satcher.html>. Accessed: 4/06/2013.
- [55] D A H Hanaor, I Chironi, I Karatchevtseva, G Triani, and C C Sorrell. Single and mixed phase TiO_2 powders prepared by excess hydrolysis of titanium alkoxide. *Advances in Applied Ceramics*, 111(3):149–158, 2012-04-01T00:00:00.
- [56] Xiaoyang Pan, Nan Zhang, Xianzhi Fu, and Yi-Jun Xu. Selective oxidation of benzyl alcohol over TiO_2 nanosheets with exposed 001 facets: Catalyst deactivation and regeneration. *Applied Catalysis A: General*, 453(0):181 – 187, 2013.
- [57] I. Chorkendorff and J.W Niemantsverdriet. *Concepts of Modern Catalysis and Kinetics*. Wiley-VCH, 2007. ISBN: 978-3-527-31672-4.
- [58] Kenneth S. Suslick. The chemical effects of ultrasound. *SCIENTIFIC AMERICAN*, 1989.

Appendix

Appendix A: Calculation examples and assumptions

Some of the copper loadings had to be converted from molar percentage to mass percentage. It was assumed for simplicity that Copper existed purely in Cu(O) form. In reality copper exists in CuO, Cu₂O and elemental Cu(O) form but the ratio of Cu species to TiO₂ is not changed when copper is oxidised which is why this assumption is acceptable.

Calculating the amount of copper, titania and water needed to produce 10 g of 10 % Cu Cu–TiO₂ photocatalyst

The copper precursor was Cu(NO₃)₂ · 3 H₂O which has a high water solubility and a molar mass of 241.6 $\frac{\text{g}}{\text{mol}}$. The total catalyst amount would be 10 g with a total copper content of 10 % on a mass basis, which means that the total mass of copper needed would be 10 g × 10 % = 1 g. The molar mass of copper is 63.546 $\frac{\text{g}}{\text{mol}}$ which means that total amount of copper precursor needed to get 1 gram of copper was $1 \times \frac{241.6 \text{ g/mol}}{63.546 \text{ g/mol}} = 3.80197 \text{ g}$. The mass of TiO₂ needed would be the remaining 90 % of the 10 g which equals 9 g. The final component of the catalyst was the water. An experiment showed that P25 titania was able to absorb around 0.893 g of water per gram powder. To make the mixture easier to work with, 20 % excess water was used which also made sure that the copper solution was evenly distributed in the P25 TiO₂. The total amount of water was then 9 × 0.893 × 1.2 = 9.6 ml.

Calculating the quantum yield

The quantum yield in this experiment is defined as the percentage of adsorbed photons that actually contributes to the reduction of H⁺ ions to H₂ gas. For this definition to be viable, one has to assume that all the photons emitted by the UV-lamps will reach the catalyst without being adsorbed by anything else. The glass reactor is transparent, the tubes are covered in aluminium foil and the outer walls are shiny which suggests that most of the UV light will actually hit the catalyst without being adsorbed. Now to the calculations:

The total radiation power is 14 UV-lamps × 8 $\frac{\text{watt}}{\text{lamp}}$ = 112 watts of power consumed to produce UV-rays. Because some light is adsorbed unwanted and the efficiency of the lamps are less than 100 %, the actual power of the UV-rays should be close to 100 watts. The very most of the rays are emitted at 254 nm which corresponds to UVC rays, but some are also at wavelengths > 390 nm making them useless to our photocatalyst. The number of photons emitted per sec is calculated this way:

$\frac{\text{photons}}{\text{second}} = \frac{\text{Energy emitted / second}}{\text{energy / photon}} = \frac{100 \text{ J/s}}{h \times \frac{c}{\lambda}}$ where planck's law $E = h \times \frac{c}{\lambda}$ is used with c as the speed of light ($3 \times 10^8 \frac{\text{m}}{\text{s}}$), h as the planck constant ($6.636 \times 10^{-34} \frac{\text{J}}{\text{s}}$) and λ as the wavelength of 254 nm. This gives 1.288×10^{20} photons/sec which corresponds to 7.7281×10^{21} photons/min. The hydrogen production rate peaked at 0.65 ml/min which had to be converted into moles by using the ideal gas law: $PV=nRT$ at atmospheric pressure and 25 °C:

$$PV = nRT \rightarrow n = \frac{RT}{PV} \rightarrow n = \frac{0.08206 \text{ L atm mol}^{-1} \text{ K}^{-1} * 298 \text{ K}}{1 \text{ atm} * 0.65 \times 10^{-3} \text{ L}} = 2.6569 \times 10^{-5} \text{ moles}$$

The peak hydrogen gas generation was at 2.6569×10^{-5} moles per minute and the quantum yield could be calculated after converting this to the number of H-atoms:

$$Q.Y = \frac{2.6569 \times 10^{-5} \frac{\text{mol H}_2}{\text{min}} * 2 \frac{\text{mol H}}{\text{mol H}_2} * 6.023 \times 10^{23} \frac{\text{H atoms}}{\text{mol H}}}{7.728 \times 10^{21} \frac{\text{photons}}{\text{min}}}$$

This gives 0,00414 $\frac{\text{reduced H atoms}}{\text{photon}}$ which multiplied by 100 % gives 0.41 % quantum yield.

Quantifying the reproducibility by calculating relative errors

Expriment #	g-cat.	Specific H2 prod. [ml/min]	Average	Error^2	Sum of errors^2	relative error [%]
1	1,001	0,66098	0,60615	0,00301	0,00514	5,916
2	1	0,56370		0,00180		
3	1	0,58856		0,00031	Standard deviation	
4	1,0002	0,61135		0,00003	0,03586	
					Sum of errors^2	
1	0,01	0,02019	0,02247	0,00001	0,00001	7,326
2	0,01	0,02322		0,00000	standard deviation	
3	0,01	0,02401		0,00000	0,00165	
					Sum of errors^2	
1	0,0245	0,18281	0,18929	0,00004	0,00008	3,425
2	0,0249	0,19577		0,00004	standard deviation	
					0,00648	

Figure 33: This is a screen-shot from the Excel worksheet where the relative errors were calculated.

The author is well aware that the number of conducted experiments are insufficient to represent a statistical basis, so these relative errors contains errors themselves (error within an error=error-ception).

Thermodynamics: Finding the temperature needed to spontaneously form significant amounts of Cu₂O

In order to investigate if any significant amounts Cu₂O was formed during calcination, the temperature at which the Gibb's free energy for conversion of CuO to Cu₂O is zero, was calculated.

compound	H _f ⁰	S ⁰						
O ₂	0	205						
Cu(NO ₃) ₂ (s)	-303							
*3H ₂ O	-1217							
*6H ₂ O	-2111							
Cu ₂ O	-169	93						
CuO	-157	43						
Cu	0	33						
NO ₂ (g)	33	240						
H ₂ O (g)	-242	189						
RX: 2CuO->Cu₂O+0.5O₂			Delta-G=Delta-H - T*(Delta-S)					
Delta-H	145							
Delta-S	152,5							
T	950,82	<----- found by goalseek, set Delta-G to "0" by changing T						
Delta-G	0							

Figure 34: This is a screen-shot from the Excel worksheet where the thermodynamics were calculated.

951 K corresponds to 951-273= 708 °C, which is far away from 200 °C. This means that practically no Cu₂O was formed at all during calcination of the photocatalyst. Note that some Cu₂O will be formed at temperatures below 950 K if equilibrium is reached, but this amount will be close to zero at a temperature as low as 200 °C.

Appendix B: List of chemicals

Table 3: The table shows a summary of the chemicals used in this project.

Chemical	Formula	Phase	Purity	Supplier
Methanol	CH_3OH	l	Analytical	VVR Chemicals
Copper(II) nitrate trihydrate	$\text{Cu}(\text{NO}_3)_2 \cdot 3\text{H}_2\text{O}$	s	$\geq 98\%$	Sigma Aldrich
Aeroxide TiO_2 P25	TiO_2	s	$\geq 99.5\%$	Evonik Degussa
Argon	Ar	g	(5.0)	Yara Praxair
Hydrogen	H	g	(5.0)	Yara Praxair

Appendix C: BET data

The raw data from the BET experiments is shown below, shown in the following order: P25, 0 % Cu, 1 % Cu, 5 % Cu and 10 % Cu.

Summary Report

Surface Area

Single point surface area at $P/P_0 = 0.300955996$: 52.5820 m²/g

BET Surface Area: 53.5569 m²/g

t-Plot Micropore Area: 0.3647 m²/g

t-Plot External Surface Area: 53.1923 m²/g

BJH Adsorption cumulative surface area of pores
between 17.000 Å and 3000.000 Å diameter: 52.122 m²/g

BJH Desorption cumulative surface area of pores
between 17.000 Å and 3000.000 Å diameter: 50.7672 m²/g

Figure 35: Raw BET data from the pure P25 sample.

Summary Report

Surface Area

Single point surface area at $P/P_0 = 0.300420148$: 52.3292 m²/g

BET Surface Area: 53.2640 m²/g

t-Plot Micropore Area: 1.1192 m²/g

t-Plot External Surface Area: 52.1447 m²/g

BJH Adsorption cumulative surface area of pores
between 17.000 Å and 3000.000 Å diameter: 53.119 m²/g

BJH Desorption cumulative surface area of pores
between 17.000 Å and 3000.000 Å diameter: 53.5323 m²/g

Figure 36: Raw BET data from the 0 % Cu sample .

Surface Area

Single point surface area at $P/P_0 = 0.301257650$: 52.2383 m²/g

BET Surface Area: 53.4703 m²/g

t-Plot External Surface Area: 55.1042 m²/g

BJH Adsorption cumulative surface area of pores
between 17.000 Å and 3000.000 Å diameter: 52.785 m²/g

BJH Desorption cumulative surface area of pores
between 17.000 Å and 3000.000 Å diameter: 51.3003 m²/g

Figure 37: Raw BET data from the 1 % Cu sample.

Surface Area

Single point surface area at $P/P_0 = 0.300999359$: 49.3297 m²/g

BET Surface Area: 49.8046 m²/g

t-Plot Micropore Area: 4.2386 m²/g

t-Plot External Surface Area: 45.5660 m²/g

BJH Adsorption cumulative surface area of pores
between 17.000 Å and 3000.000 Å diameter: 48.541 m²/g

BJH Desorption cumulative surface area of pores
between 17.000 Å and 3000.000 Å diameter: 48.8038 m²/g

Figure 38: Raw BET data from the 5 % Cu sample.

Surface Area

Single point surface area at $P/P_0 = 0.300466792$: 44.2522 m²/g

BET Surface Area: 44.7463 m²/g

t-Plot Micropore Area: 3.7292 m²/g

t-Plot External Surface Area: 41.0171 m²/g

BJH Adsorption cumulative surface area of pores
between 17.000 Å and 3000.000 Å diameter: 44.891 m²/g

BJH Desorption cumulative surface area of pores
between 17.000 Å and 3000.000 Å diameter: 44.4857 m²/g

Figure 39: Raw BET data from 10 % Cu sample.

Appendix D: HSE and risk assessment

Explanation of the Risk Matrix



What's A Risk Matrix

A risk matrix is simple graphical tool. It provides a process for combining the chance for an occurrence of an event (likelihood) and the consequence if the event occurred. Use the tool for everyday judgements and decisions.

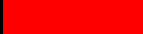


Know when to accept the risk. Know when to reject the risk.

Just for information!
Do not write in this form.

RISK ASSESSMENT MATRIX

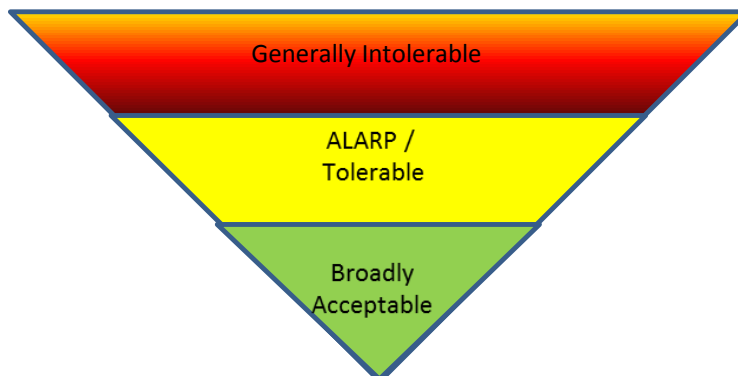
		Column1	Column2	Column3	Column4	Column5	Column6
CONSEQUENCE	Very critical	E1	E2	E3	E4	E5	
	Critical	D1	D2	D3	D4	D5	
	Dangerous	C1	C2	C3	C4	C5	
	Relative safe	B1	B2	B3	B4	B5	
	Safe	A1	A2	A3	A4	A5	
		Minimal	Low	Medium	High	Very high	
	LIKELIHOOD						

Risk Increases In This Direction

COLOR	Describing function	
Red		Extreme risk – immediate action required
Yellow		Attention needed to develop risk reduction strategies.
Green		Minimal injury requiring no/minimal intervention or treatment.

ALARP

Risk will be treated to ensure they are "As Low As Reasonably Practical"(ALARP) or in the "Broadly Acceptable" areas.



Potential undesirable incident/strain

Identify possible incidents and conditions that may lead to situations that pose a hazard to people, the environment and any materiel/equipment involved.

Criteria for the assessment of likelihood and consequence in relation to fieldwork


Each activity is assessed according to a worst-case scenario. Likelihood and consequence are to be assessed separately for each potential undesirable incident. Before starting on the quantification, the participants should agree what they understand by the assessment criteria:


Minimal 1	Low 2	Medium 3	High 4	Very high 5
Once every 50 years or less	Once every 10 years or less	Once a year or less	Once a month or less	Once a week



Likelihood

Grading	Human	Environment	Financial/material
E Very critical	May produce fatality/ies	Very prolonged, non-reversible damage	Shutdown of work >1 year.
D Critical	Permanent injury, may produce serious health damage/sickness	Prolonged damage. Long recovery time.	Shutdown of work 0.5-1 year.
C Dangerous	Serious personal injury	Minor damage. Long recovery time	Shutdown of work < 1 month
B Relatively safe	Injury that requires medical treatment	Minor damage. Short recovery time	Shutdown of work < 1 week
A Safe	Injury that requires first aid	Insignificant damage. Short recovery time	Shutdown of work < 1 day

Consequence

NTNU		Hazardous activity identification process		Prepared by	Number	Date
				HSE section	HMSRV2601	17.01.2013
HMS				Approved by	Page	
			The Rector	1 out of 1		
Unit: IKP		Date: 17.01.2013				
Participants in the identification process (including their function):						
Eirik Djuve (student), Magnus Rønning (supervisor), Charitha Udini (co-supervisor)						
Short description of the main activity/main process: Synthesis of photocatalysts						
ID no.	Activity/process	Responsible person	Laws, regulations etc.	Existing documentation	Existing safety measures	Comment
S1	Degussa P25 TiO ₂ handling	Magnus Rønning	AML §4-5, HMSRV-12/13, HMSR-39, HMSR-40, Kjemikalieforskriften	Material safety data sheet	Closed fume hood	Safety goggles, gloves, lab coat
S2	Copper(II) nitrate handling	Magnus Rønning	AML §4-5, HMSRV-12/13, HMSR-39, HMSR-40, Kjemikalieforskriften	Material safety data sheet	Closed fume hood	Safety goggles, gloves, lab coat
S3	Calcination	Magnus Rønning	AML §4-5, HMSRV-12/13, HMSR-39, HMSR-40, Kjemikalieforskriften	Manuals	Closed fume hood	Safety goggles, thermo gloves, lab coat

NTNU		Hazardous activity identification process		Prepared by	Number	Date
				HSE section	HMSRV2601	17.01.2013
HMS				Approved by	Page	
				The Rector	1 out of 1	
Unit:	IKP	Date:	17.01.2013			
Participants in the identification process (including their function):						
Eirik Djuve (student), Magnus Rønning (supervisor), Charitha Udini (co-supervisor)						
Short description of the main activity/main process: Photoreforming of methanol						
ID no.	Activity/process	Responsible person	Laws, regulations etc.	Existing documentation	Existing safety measures	Comment
P1	Activity measurements using UV-light	Magnus Rønning	HMSR-32, strålevernloven, strålevernforskriften, manualer, prosedyrer	Material safety data sheet, manuals	Use UV-protecting goggles	
P2	Handling of methanol	Magnus Rønning	AML §4-5, HMSRV-12/13, HMSR-39, HMSR-40, Kjemikalieforskriften	Material safety data sheet	Closed fume hood	Safety goggles, gloves, lab coat
P3	Hydrogen gas usage in GC calibration and reactivation	Magnus Rønning	AML §4-5, HMSRV-12/13, HMSR-39, HMSR-40, Kjemikalieforskriften	Material safety data sheet	Use of handheld Gas detectors	

NTNU	Risk assessment			Prepared by	Number	Date
				HSE section	HMSRV2601	17.01.2013
HMS /KS				Approved by	Page	
		The Rector	1 out of 1			



Unit: IKP

Date: 17.01.2013

Participants in the identification process (including their function):

Eirik Djuve (student), Magnus Rønning (supervisor), Charitha Udini (co-supervisor)

ID no.	Activity from the identifica	Potential undesirable incident/strain	Likelihood:		Consequence:		Risk value	Comments/status Suggested measures
			Likelihood (1-5)	Human (A-E)	Human (A-E)	Reputation (A-E)		
P1	Activity measurements using UV-light	Exposure to UV radiation	5	A			Human	Skin is exposed for max 10 sec. a day
P2	Handling of methanol	Spilling and splashing	4	A			Human	Use goggles, gloves and lab coat
P3	Hydrogen gas usage in GC calibration and reactivation	Gas leakage, explosion	1	D			Human	Use gas detectors at all times
S1	Degussa P25 TiO2 handling	Innhalation of dust	3	A			3A	Keep it away from airways
S2	Copper(II) nitrate handling	Skin exposure	1	B			1B	Use gloves
S3	Calcination	Heat exposure and gas leakage	2	B			2B	Wait for cooling, use thermogloves
7								
8								

NTNU	Risk assessment			Prepared by	Number	Date
				HSE section	HMSRV2601	17.01.2013
HMS/KS				Approved by	Page	
			The Rector	1 out of 1		

Unit: IKP Date: 17.01.2013

Participants in the identification process (including their function):

Eirik Djuve (student), Magnus Rønning (supervisor), Charitha Udini (co-supervisor)

ID no.	Activity from the identification	Potential undesirable incident/strain	Likelihood:		Consequence:		Risk value	Comments/status Suggested measures
			Likelihood (1-5)	Human (A-E)	Human (A-E)	Reputation (A-E)		
P1	Activity measurements using UV-light	Exposure to UV radiation	5	A			Human	Skin is exposed for max 10 sec. a day
P2	Handling of methanol	Spilling and splashing	4	A			4A	Use goggles, gloves and lab coat
P3	Hydrogen gas usage in GC calibration and reactivation	Gas leakage, explosion	1	D			1D	Use gas detectors at all times
S1	Degussa P25 TiO2 handling	Inhalation of dust	3	A			3A	Keep it away from airways
S2	Copper(II) nitrate handling	Skin exposure	1	B			1B	Use gloves
S3	Calcination	Heat exposure and gas leakage	2	B			2B	Wait for cooling, use thermogloves
7								
8								

SIKKERHETSDATBLAD
Forkortet versjon
(Lenk til fullversjon nedenfor)

COPPER(II) NITRATE
HEMI(PENTAHYDRATE),
PURISS. P.A., ACS REAGENT,
99-102 %

URL for fullversjon av Sikkerhetsdatablad	http://www.sigma-aldrich.com/MSDSLlookup.html?ProdNo=31288...
Utgitt dato	11.02.2006
Kjemikaliets navn	COPPER(II) NITRATE HEMI(PENTAHYDRATE), PURISS. P.A., ACS REAGENT, 99-102 %
CAS-nr.	19004-19-4
Artikkelnr.	31288
Firmanavn	Sigma-Aldrich Norway AS
Postadresse	Tevlingv 23
Postnr.	1011
Poststed	Oslo
Land	NORGE
Telefon	23176000
Telefaks	23176010
E-post	eurtechserv@sial.com
Hjemmeside	http://www.sigma-aldrich.com/norway

Faresymbol



R-setninger	8-22-34
S-setninger	17-26-36/37/39-45
Endret	13.03.2007

SIKKERHETSDATABLAD

Forkortet versjon (Lenk til fullversjon nedenfor)

Metanol

Seksjon 1: Identifikasjon av stoffet / blandingen og av selskapet / foretaket

URL for fullversjon av Sikkerhetsdatablad	http://www.sigma-aldrich.com/MSDSLlookup.html?ProdNo=32241...
Opplastet fullversjon av Sikkerhetsdatablad	Metanol.pdf
Utgitt dato	18.05.2006
Revisjonsdato	08.02.2013

1.1. Produktidentifikasjon

Kjemikaliets navn	Metanol
Synonymer	METHANOL, ANHYDROUS, 99.8 %
REACH reg. nr.	01-2119433307-44-XXXX
CAS-nr.	67-56-1
Indeksnr.	603-001-00-X
Artikkelnr.	322415 (Sigma-Aldrich)

1.2. Relevant identifiserte bruksområder for stoffet eller blandingen og bruk det frarådes mot

Kjemikaliets bruksområde	Laboratoriekjemikalier, Produksjon av stoffer
--------------------------	---

1.3. Nærmere opplysninger om leverandøren av sikkerhetsdatabladet

Firmanavn	Sigma-Aldrich Norway AS
Postadresse	Tevlingv 23
Postnr.	1011
Poststed	Oslo
Land	NORGE
Telefon	23176000
Telefaks	23176010
E-post	eurtechserv@sial.com
Hjemmeside	http://www.sigma-aldrich.com/norway

1.4. Nødtelefon

Nødtelefon	Giftinformasjonssentralen:22 59 13 00
------------	---------------------------------------

Seksjon 2: Fareidentifikasjon

2.1. Klassifisering av stoff eller blanding

2.2. Etikettinformasjon

Farepiktogrammer (CLP)



Signalord	Fare
Faresetninger	H225 Meget brannfarlig væske og damp. H301 Giftig ved svelging. H311 Giftig ved hudkontakt. H331 Giftig ved innånding. H370 Forårsaker organskader.
Sikkerhetssetninger	P210 Holdes vekk fra varme/gnister/åpen flamme/varme overflater. - Røyking forbudt. P260 Ikke innånd støv /røyk/ gass/ tåke/ damp/ aerosoler. P280 Benytt vernehansker/ verneklær. P301 + P310 VED SVELGING: Kontakt umiddelbart et GIFTINFORMASJONSSENTER eller lege. P311 Kontakt et GIFTINFORMASJONSSENTER eller lege.

2.3 Andre farer

Seksjon 3: Sammensetning / opplysning om innholdsstoffer

3.2. Blandinger

Seksjon 4: Førstehjelpstiltak

4.1. Beskrivelse av førstehjelpstiltak

Generelt	Kontakt lege. Vis dette sikkerhetsdatabladet til tilstedeværende lege.
Innånding	Ved innånding, fjern personen til frisk luft. Hvis den forulykkede ikke puster, gi kunstig åndedrett. Kontakt lege.
Hudkontakt	Vask med såpe og mye vann. Pasienten bringes omgående til sykehus. Kontakt lege.
Øyekontakt	Skyll grundig med rikelig med vann i minst 15 minutter og kontakt lege.
Svelging	Fremkall IKKE brekninger. Gi aldri noe gjennom munnen til en bevisstløs person. Skyll munnen med vann. Kontakt lege.

4.2. Viktigste symptomer og effekter, både akutt og forsinket

Informasjon til helsepersonell	De viktigste kjente symptomer og virkninger er beskrevet i merking (se avsnitt 2.2), og / eller i avsnitt 11
--------------------------------	--

4.3. Informasjon om umiddelbar legehjelp og spesiell behandling som eventuelt er nødvendig

Seksjon 5: Tiltak ved brannslukning

5.1. Brannslukningsmidler

Passende brannslukningsmidler	Bruk vannspray, alkoholresistent skum, tørrkemikalier eller karbondioksid.
-------------------------------	--

5.2. Spesielle farer som stoffet eller blandingen kan medføre

Brann- og eksplosjonsfarer	Spesielle farer som kommer fra stoffet eller blandingen Karbonoksider
----------------------------	--

5.3. Anvisninger for brannmannskaper

Personlig verneutstyr	Bruk om nødvendig trykkluftmaske ved brannslukning.
Brannslukningsmetoder	Vannspray kan brukes for å avkjøle uåpnede beholdere.

Seksjon 6: Tiltak ved utilsiktet utslipp

6.1. Personlige forholdsregler, verneutstyr og nødprosedyrer

Generelle tiltak	Bruk åndedrettsvern. Unngå innånding av damp, tåke eller gass. Sørg for skikkelig ventilasjon. Alle tennkilder fjernes. Evakuer personalet til sikkert område. Vis forsiktighet for oppsamling av damper som danner eksplosive
------------------	--

konsentrasjoner. Damp kan samles på lave områder. For personlig beskyttelse, se seksjon 8.

6.2. Sikkerhetstiltak for å beskytte ytre miljø

Sikkerhetstiltak for å beskytte ytre miljø Forhindre ytterligere lekkasje eller søl dersom det er forsvarlig. Forhindre utslipp til avløpsystemet.

6.3. Metoder for opprydding og rengjøring

Metoder for opprydding og rengjøring Oppbevar og samle spill med en elektrisk beskyttet støvsuger eller ved våt-børsting og plasser i beholder for avskaffelse i henhold til lokale bestemmelser (se seksjon 13).

6.4. Referanse til andre seksjoner

Seksjon 7: Håndtering og lagring

7.1. Forholdsregler for sikker håndtering

Håndtering Unngå kontakt med huden og øynene. Unngå innånding av damp eller tåke. Holdes vekk fra antennelseskilder - Røyking forbudt. Ta forholdsregler for å forhindre oppbygging av elektrostatisk ladning. For forholdsregler se avsnitt 2.2.

7.2. Betingelser for sikker oppbevaring, inklusiv eventuelle uforenligheter

Oppbevaring Lagre på en kjølig plass. Hold beholderen tett lukket på et tørt og godt ventilert sted. Åpne beholdere må lukkes med forsiktighet og lagres i oppreist stilling for å hindre lekkasje.

7.3 Spesifikk bruk

Anbefalinger Bortsett fra bruksområdene nevnt i avsnitt 1.2 er det ikke andre spesifikke bruksområder foreskrevet

Seksjon 8: Eksponeringskontroll / personlig verneutstyr

8.1. Kontrollparametere

8.2 Begrensning av eksponering på arbeidsplassen

Begrensning av eksponering på arbeidsplassen Unngå kontakt med hud, øyne og klær. Vask hendene før arbeidspauser og med en gang etter å ha håndtert stoffet.

Åndedrettsvern

Åndedrettsvern Når risikovurdering viser at luftrensende åndedrettsvern er hensiktsmessig, bruk helmaske, med flerbrukskombinasjonsfilter eller type AXBEK-filter (EN 14387) som støtte til eksterne ventilasjonssystemer. Dersom åndedrettsvern er den eneste beskyttelsen, bruk luftforsynt åndedrettsvern med helmaske. Bruk åndedrettsvern og komponenter som er testet og godkjent etter standarder som NIOSH (US) eller CEN (EU).

Håndvern

Håndvern Håndteres med vernehansker. Hansker må inspiseres før bruk. Bruk riktig teknikk ved fjerning av hansker (uten å berøre hanskens overflate) for å unngå hudkontakt med dette produktet. Kast forurensede hansker etter bruk i henhold til gjeldende lover og god laboratoriepraksis. Vask og tørk hendene. De valgte vernehanskene må tilfredsstillende spesifikasjonene til EU Direktiv 89/686/EØF og standarden EN 374 derivert fra direktivet.
Full kontakt:
Materiale: butylgummi
minimum hansketykkelse: 0,3 mm
Gjennomtrengningstid: 480 min
Materiale testet: Butoject® (KCL 897 / Aldrich Z677647, Størrelse M)
Sprut:
Materiale: Nitrilgummi

minimum hanskeykkelse: 0,4 mm
Gjennomtrengningstid: 31 min
Materiale testet: Camatril® (KCL 730 / Aldrich Z677442, Størrelse M)
datakilde: KCL GmbH, D-36124 Eichenzell, Telefon +49 (0)6659 87300, e-mail sales@kcl.de,
testmetode: EN374
Dersom de brukes i oppløsningsmidler eller blandes med andre stoffer og under forhold som ikke dekkes av EN 374, ta kontakt med leverandøren til de EF godkjente hanskene. Denne anbefalingen er bare rådgivende, og bør vurderes av ansvarlig kjemiker, som kjenner den forventede bruk. Dette skal ikke oppfattes som en godkjenning av ethvert bruksscenario.

Øye- / ansiktsvern

Øyevern Ansiktsvern og vernebriller Bruk utstyr for øyebeskyttelse som er testet og godkjent i henhold til standarder som NIOSH (US) og EN 166 (EU).

Hudvern

Annet hudvern enn håndvern Komplette drakt for beskyttelse mot kjemikalier, Flammehemmende antistatisk kledning, Typen av verneutstyr må velges i henhold til konsentrasjonen og mengden av det farlige stoffet på arbeidsplassen.

Seksjon 9: Fysiske og kjemiske egenskaper

9.1. Informasjon om grunnleggende fysiske og kjemiske egenskaper

Tilstandsform	væske
Farge	fargeløs
Lukt	påtrengende
Smeltepunkt/smeltepunktintervall	Verdi: -98 °C
Kokepunkt / kokepunktintervall	Verdi: 64,7 °C
Flammepunkt	Verdi: 9,7 °C

9.2 Annen informasjon

Seksjon 10: Stabilitet og reaktivitet

10.1. Reaktivitet

10.2. Kjemisk stabilitet

10.3. Risiko for farlige reaksjoner

10.4. Forhold som skal unngås

10.5. Materialer som skal unngås

10.6 Farlige spaltningsprodukter

Seksjon 11: Toksikologisk informasjon

11.1 Informasjon om toksiologiske effekter

Seksjon 12: Miljøopplysninger

12.1. Toksisitet

12.2. Persistens og nedbrytbarhet

12.3. Bioakkumulasjonspotensial

12.4. Mobilitet i jord

12.5. Resultater av PBT og vPvB vurdering

12.6. Andre skadevirkninger

Seksjon 13: Fjerning av avfall

13.1. Metoder for avfallsbehandling

Seksjon 14: Transportinformasjon

14.1. UN-nummer

14.2. UN varenavn

14.3. Transport fareklasse

14.4. Emballasjegruppe

14.5. Miljøfarer

14.6. Spesielle forholdsregler for bruker

14.7. Transport i bulk i henhold til vedlegg II til MARPOL 73/78 og IBC-koden

Seksjon 15: Opplysninger om lover og forskrifter

Faresymbol



R-setninger

R11 Meget brannfarlig.
R23/24/25 Giftig ved innånding, hudkontakt og svelging.
R39/23/24/25 Giftig: fare for alvorlig varig helseskade ved innånding, hudkontakt og svelging.

15.1. Forskrift / regelverk om stoff eller blanding i forhold til sikkerhet, helse og miljø

15.2. Vurdering av kjemikaliesikkerhet

Seksjon 16: Andre opplysninger

Ansvarlig for Sikkerhetsdatablad

Sigma-Aldrich Norway AS